Chapter 13
Thermal Damage and Rate Processes in Biologic Tissues

Sharon Thomsen and John A. Pearce

13.1 Introduction

Heat is generated in laser irradiated tissues by absorption and transformation of the light energy into heat. Once generated within tissues, heat is heat no matter what original energy source is used to produce it. Heating of cells and biological tissues can produce reversible injury and dysfunction that can be repaired by innate cellular and host mechanisms. However, more severe, irreversible damage leads to death immediately (primary thermal effects) or after (delayed secondary effects) the heating event. Sometimes, the dividing line between reversible (repairable) and irreversible (lethal) damage in living, surviving tissues is not easily observed at the time of heating. Therefore, to determine accurately the extent of effective (killing) thermal treatment, the observer has to wait for all the moribund, injured cells to die and undergo post-mortem necrosis (two-four days) [1–6]. In addition, low temperature heat can directly trigger cell death by apoptosis, a sequential series of complicated processes that requires energy, signal transduction, enzyme activation and time (hours to days) to develop [6–9].

The effects of cellular and tissue heating can be studied using both qualitative and quantitative gross and microscopic pathologic methods. Some of these effects are characteristic of direct thermal damage, but others are delayed non-specific responses and thus are attributable to thermal injury only when a history of thermal damage is provided.

In this chapter, the qualitative and quantitative pathologic markers of thermal damage will be identified, described and illustrated. In addition, experimental and computational methods will be described for estimating kinetic coefficients for those particular markers that develop as a result of physical and chemical reactions that can be described by first-order kinetics. The experimental results can be obtained under constant temperature or transient thermal history situations simulating continuous and pulsed laser irradiations. To be useful for the prediction

S. Thomsen (✉)
500 Discovery View Drive, Sequim, WA, USA
e-mail: slthomsenmd@yahoo.com

A.J. Welch, M.J.C. van Gemert (eds.), *Optical-Thermal Response of Laser-Irradiated Tissue*, 2nd ed., DOI 10.1007/978-90-481-8831-4_13,

of these temperature/time treatment dosimetries, the kinetic model must be coupled to quantitative pathological analyses of well-defined pathologic end points showing thermal effects. For many heat treatment clinical goals that involve cell killing, the more useful endpoints are the spatial boundaries of (1) cell and tissue death (effective treatment volume) and (2) full extent of the lethal and non-lethal thermal effects (total treatment volume). In the case of in vivo experiments with transient thermal histories, the experimental data yield a noisy kinetic plot; however, good estimates of the appropriate rate coefficients can be made using a relatively new method described in Section 13.3.

13.2 Pathophysiology and Pathogenesis of Photothermal Lesions

13.2.1 General Principles

13.2.1.1 Primary Thermal Injury

Pathologic mechanisms of primary thermal injury are those that produce acute structural and functional abnormalities in cells and tissues due to the *direct physical interaction* of the heat with cellular and tissue proteins, lipoproteins and water. These pathologic effects can be detected immediately, during, or just after the heating episode in either living tissues (in vivo), living cells in culture (in vitro), or non-living tissues or organs recently removed from animals (ex vivo). The most characteristic and reliable diagnostic histopathophysiologic markers (indicators) of thermal injury are those produced by primary mechanisms of pathologic effects (see Table 13.1).

13.2.1.2 Secondary (Delayed) Thermal Injury

Pathologic mechanisms of secondary (delayed) thermal injuries are based on *delayed pathophysiologic cellular, tissue or host responses* triggered by cellular and tissue injuries and/or death. These secondary pathologic responses can occur soon (several seconds, minutes or hours) or long (days, weeks or months) after the heating event. Therefore, the full story of the development, progression and resolution (healing) of photothermal lesions can only be studied in living and surviving cells, tissues and organisms (see Table 13.2). These delayed responses are not unique to thermal lesions but are characteristic of the cellular and host reactions to any chemical, mechanical or physical insult that results in reversible and irreversible (lethal) cellular and tissue injury [6].

13.2.1.3 Identification of Thermal Lesions

The determination that a lesion is due to thermal injury requires (1) the observation of characteristic (diagnostic) pathologic markers of thermal damage (mainly

primary effects) in the tissues, (2) having the history of a heating episode and/or (3) the documentation of the heating parameters (tissue temperature and time at temperature) to show that significant heat injury could have been produced in that tissue or organ. Satisfaction of at least two or all three of these criteria is necessary to establish the role of heat in the creation of the lesion.

Table 13.1 Primary thermal effects in non-viable and viable tissue targets: low to high temperature sequence

In Vitro/Ex Vivo/In Vivo
I. *Thermal Activation of Increased Mitochondrial Membrane Permeability of Ions*
II. *Thermal Dissociation (Melting) of Phospholipid Cellular Membranes*
• Rupture of cellular and intracellular membranes • Loss of transmembrane electrical potentials • Leakage of cellular contents including water, ions and micro and macromolecules • Increasing disruption of functional arrays of membrane-associated enzymes & proteins
III. *Thermal Intracellular Protein Denaturation*
• Vital (Respiratory) mitochondrial enzymes • Membrane-associated receptor, transport and signal processing proteins • Metabolic and synthetic enzymes • Protein secretory products • Other intracellular and extracellular non-structural proteins, lipoproteins and glycoproteins • Intracellular nuclear and cytoplasmic structural proteins
IV. *Thermal Extracellular Stromal Protein Denaturation*
• Loss of tertiary and secondary molecular structure and associated physiologic functions • Severe intracellular and extracellular protein denaturation and precipitation in situ (heat fixation)
V. *Water Vaporization*
• Tissue desiccation • Accumulation of water vapor in expanding tissue vacuoles
VI. *Tissue Caramelization and Carbonization*
VII. *Tissue Ablation*
• Rupture of thin-walled vacuoles with explosive fragmentation of desiccated tissue • Tissue combustion • Tissue vaporization • Tissue plasma formation

Modified from [4]

Table 13.2 Secondary (delayed) thermal effects: pathologic responses to cell and tissue injury and death

In vivo and survival only: local host responses	In vivo and survival only: cellular and tissue responses	In vivo and survival only: host responses
I. *Red Thermal Vascular Damage Zone (Transition Zone*)* • Hemostasis • Thrombosis • Hemorrhage • Hyperhemia	II. *Cellular Repair (Non-lethal Injury)* • Reconstitution of cellular membranes • Heat shock protein production • Resumption of cellular synthetic and physiologic functions III. *Traumatic Cell and Tissue Death* • Lytic necrosis due to release of lytic enzymes from thermally damaged intracellular organelles (lysosomes) • Coagulative cell necrosis due to loss of energy production in thermally damaged mitochondria • Ischemic (coagulative) necrosis due to regional blood flow blockage (infarction) IV. *Cell Death Due to Apoptosis*	V. *Inflammatory Response to Tissue Death and Necrosis* • Release of local cytokines, cytotactic factors and vascoactive factors • Activation of cell attachment receptors • Activation of immune responses VI. *Organization of Necrotic Debris* VII. *Tissue Regeneration and Repair* • Parenchymal cellular regeneration • Wound healing: vascular and fibrous granulation tissue formation Fibrous scar maturation Fibrous scar contraction

Modified from [4]
*Transition Zone. Described by J. Coad in [10]

13.2.1.4 Factors Associated with Thermal Lesion Size, Development and Progression

The extent and severity of the pathologic effects produced by the interactions of heat with biologic tissue are determined by (1) the geometry of the heat source volume and thermal gradients created in the tissue over time, (2) tissue optical and thermal properties before heating and their dynamic changes during and after heating, (3) tissue temperatures and time at temperature (thermal history) at any point along the thermal gradients, (4) target tissue composition and structure including protein, lipid and water content and their structural anatomy, (5) target tissue viability, (6) mechanisms of primary (direct) and secondary (delayed) thermal injury, and (7) the various cellular, tissue and host responses to the injury over time in surviving organisms. The signals for these responses involve the release of several soluble

tissue cytokines, cytotactic factors and growth factors from (1) injured, dying and/or necrotic cells, (2) invading inflammatory cells, and (3) surrounding viable parenchymal and connective tissue cells. Usually, these factors are various polypeptides that can trigger (1) local vascular and cellular inflammatory events, (2) immune responses, and (3) control regional cell proliferation and protein synthesis over time [6, 10–13].

13.2.1.5 Cells: Basic Units of Life and Death

In general, when considering lethal thermal injury of tissues, it is good to remember that individual cells are the basic unit of life. All tissues and organs are a mixture of *living* cells residing in a more heat resistant, *non-living* extracellular matrix. The extracellular matrix is a structurally and functionally complex tangle of formed and unformed proteins such as collagens, elastins, glycoproteins, globular proteins and polypeptides suspended in a solution of water, sugars and salts. The more formed matrix elements such as the collagens, elastin and basement membranes are arranged into a scaffolding of support platforms and compartments to provide the functional organization for parenchymal cells and tissues such as glands, skin, nerves, muscle and bone. The matrix components are produced and maintained by living cells within the tissue including parenchymal cells (epithelial, muscle and nerve cells) and connective tissue cells such as fibroblasts, lipocytes and myofibrocytes [14–18].

At low temperatures and heating times, individual tissue cells can die, but the extracellular matrix remains intact leaving a preformed scaffolding to guide regenerating parenchymal cells into reconstituted, functioning structures such as glandular ducts and liver lobules. However, when higher temperatures and longer heating times are applied, then the scaffolding collapses and the whole necrotic tissue is replaced by scar tissue. Also, if the rate of formation of scar tissue is greater than that of parenchymal cell regeneration, the volume of the necrotic tissue will be filled by scar rather than regenerating parenchyma. These rates vary greatly among different species and among different tissues within the same species [19].

13.2.2 Zones of Thermal Damage: Gross and Histologic Pathologic Features

13.2.2.1 Heat Source Volumes and Thermal Gradients

The geometry of the heat source volume in laser irradiation is determined by the volume distribution of the absorbed light and the transformation of the absorbed light energy to heat [20, 21]. Initially, heat energy is confined to the light absorbing tissue volume. But, over time, temperature gradients between the heated source volume and the cooler peripheral tissues will be produced by the radial and axial transport of the heat energy away from the original heat source volume. Heat produces many

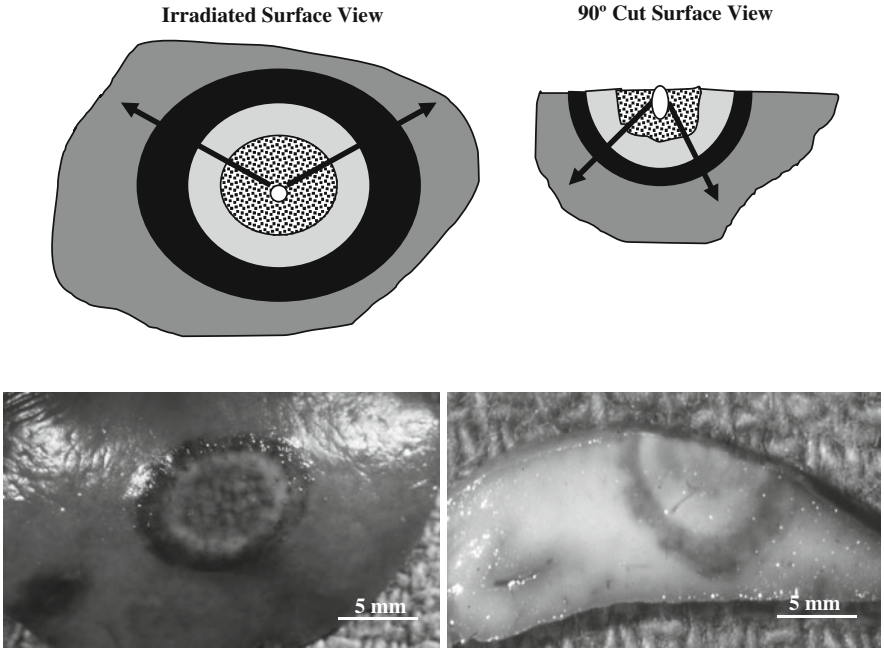

Fig. 13.1 Thermal lesions in living and surviving biologic tissue. *Top*: Schematic views of acute thermal lesions. Heat gradients (*arrows*) extend radially from a single volume heat source ◯ into the peripheral tissues. The different bands represent the concentric zones of thermal damage that form at the hottest point in the center to the cooler periphery. *Bottom*: Similarly oriented views of acute photothermal lesions in rat liver exposed in vivo to cw Nd:YAG laser irradiation (λ =1.064 μ; beam spot size, 2 mm; 9 W, 10 s). Harvested 30 min after irradiation and fixed in 10% buffered formalin. The boundaries of the different concentric thermal damage zones are distinct. The inner mottled zone and the more peripheral homogenous light zone represent different severities of thermal protein denaturation (thermal coagulation), i.e. primary thermal injury. The most peripheral darker zone represents vascular-based responses to heat, i.e. secondary thermal injury

pathological lesions within biologic tissues depending on the tissue temperature $T(r, t)$ and time at temperature $t(r, T)$ at any point along the gradients. These pathologic lesions will form concentric zones of thermal damage around the single volume heat source with the more severe effects found closer to the hot center and less severe in the cooler periphery (Fig. 13.1). Since many of these zones are separated by distinct boundaries, the pathologic effects of heating can not only be recognized and described (qualitative pathology), but also their boundaries can be measured and mapped (quantitative pathology). These data can be used to generate mathematical models of thermal effects in tissues as discussed in Section 13.3 [3, 10, 19, 22, 23].

13.2.2.2 Ex Vivo and In Vivo Heating: No Survival

Beginning at the hot center and progressing to the cooler periphery, the thermal damage zones include (1) tissue defects due to tissue ablation, (2) carbonization, (3) water vaporization, (4) thermal tissue and cellular protein coagulation or denaturation, and (5) cellular and intracellular organelle lipoprotein membrane rupture and collapse. All of these primary pathological effects reflect heating conditions sufficient to cause lethal thermal injury, that is, injury leading to cell death in living tissues and organs. All these pathologic zones can be created in recently extracted, fresh (ex vivo) and living (in vivo) tissues and organs.

13.2.2.3 In Vivo Heating with Short Term Survival

However, other pathologic lesions resulting from heating require that the host animals are alive, have an intact blood supply and blood pressure and survive at least for several seconds to a few hours after the heating event (Fig. 13.2). Thermal protein denaturation, cellular membrane damage and endothelial cell death by apoptosis produces blood vessel damage that results in a red thermal zone of vascular damage at the interface of the thermal lesion and the surrounding normal tissue.

Depending on the irradiation/heating conditions, the outer boundary of this red damage zone usually marks the outer boundary of cell/tissue death [2, 3, 19]. However, the repair mechanisms of some viable, yet heat-injured cells located at the cooler, outer edges of the red zone may remain intact. These individual cells can repair themselves and survive. Therefore, for heat treatments of invasive cancers, standard practice involves creating an additional therapeutic margin of 5–10 mm around the tumor to make sure that the thermal treatment volume encompasses as many invading cancer cells as possible.

13.2.2.4 In Vivo Heating with Prolonged Survival

Upon prolonged survival (hours to months), the host response to lethal thermal injury will involve a series of pathophysiological events that are triggered by any injurious insult to living cells and tissues, not just heat. Initially, these non-specific, general responses include post-mortem cell and tissue necrosis (Fig. 13.3). Then, resolution and repair of the tissue structural and functional void left by the necrotic process involves (1) organization, that is, clean up and removal of necrotic debris soon followed by (2) tissue repair that includes tissue regeneration and wound healing (scar formation) (see Figs. 13.6, 13.7, 13.8, and 13.9).

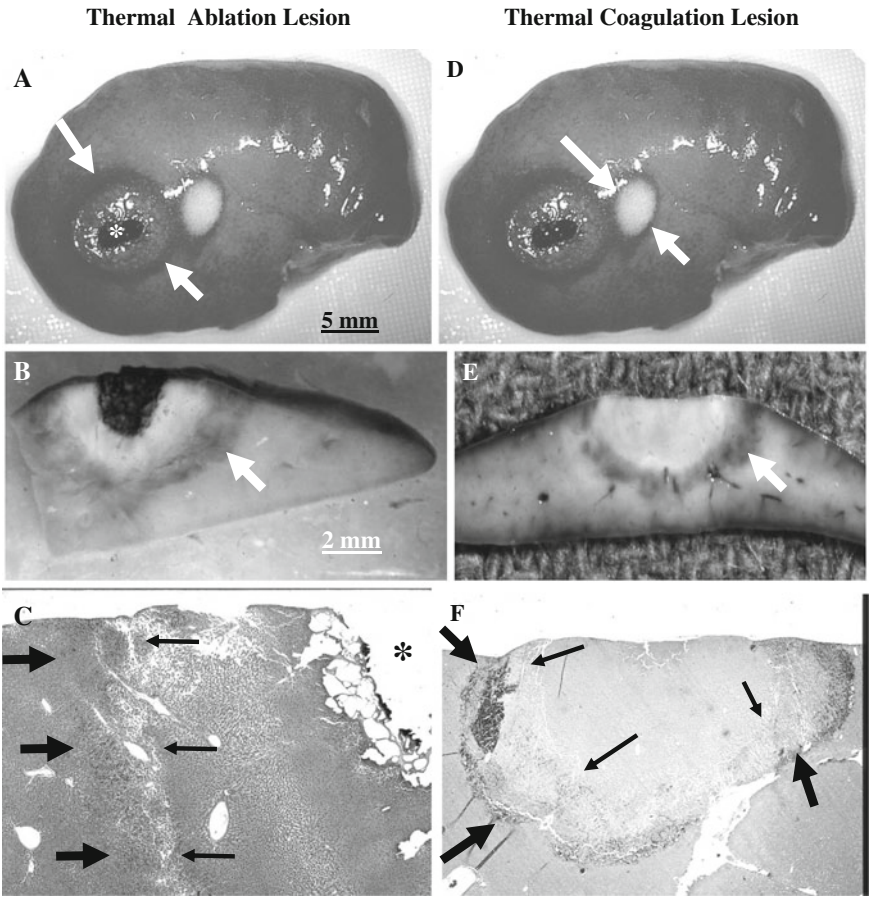

Fig. 13.2 Photothermal lesions in rat liver surviving 30 min after irradiation (cwNdYAG laser; $\lambda = 1.064$ μ: beam spot size, 2 mm; 9 W, 10 s). (**a**) Ablation lesion: irradiated surface, fresh specimen, gross appearance: black carbon deposits line the ablation hole (*asterisk*) that is surrounded by mottled, thermally denatured (coagulated) tissue. A distinct darker rim of thermal vascular damage (*arrows*) defines the periphery of the heat lesion. (**b**) Ablation lesion. cut surface, 10% formalin fixed gross specimen: The ablation hole is lined by a thin layer of dark carbonized tissue and surrounded by a prominent zone of lightly colored, thermally coagulated liver tissue and, more peripherally, a darker band of tissue (*arrow*) distorted by vascular thermal damage. (**c**) Ablation lesion. Microscopic section: a distinct zone of vacuoles formed by entrapment of water vapor in desiccated tissue is located just below the thin black carbon deposits that line the ablation hole (*asterisk*). The next zone is formed of thermally denatured (coagulated) tissues and, more peripherally, the outer zone is the band of red vascular thermal damage (*arrows*). The tissue beyond the red zone is normal, viable liver tissue. (Hematoxylin and eosin, H and E, stains. Original Magnification 25×). (**d**) Thermal coagulation lesion. Gross appearance: thermal denaturation (thermal coagulation) of the numerous tissue proteins and other macromolecules produce a white, opaque, firm central lesion surrounded by a distinct dark band of thermal vascular damage (*arrows*). (**e**) Thermal coagulation lesion. Cut surface, 10% buffered formalin fixed gross specimen: The zone boundaries demarcating the central zone of light tan, thermally coagulated liver, the more peripheral dark band of thermal vascular damage (*arrow*) and the outer non-damaged

Fig. 13.2 (continued) viable liver are distinct. (**f**) Thermal coagulation lesion. Microscopic appearance: The entire central zone of thermal denaturation (thermal coagulation) appears homogeneous at this low magnification. The more peripheral thermal vascular damage zone (*arrows*) appears more spotty and irregular in this 4 μ thick tissue section than in the gross lesion. The thermal vascular damage zone is dark because of primary heat fixation of red blood cells within their blood vessels, hemorrhage (blood escaping through the walls of heat damaged blood vessels, thrombosis (intravascular blood coagulation) and hyperhemia (increased blood flow through dilated blood vessels). (H and E stains. Orig. Mag. 16×)

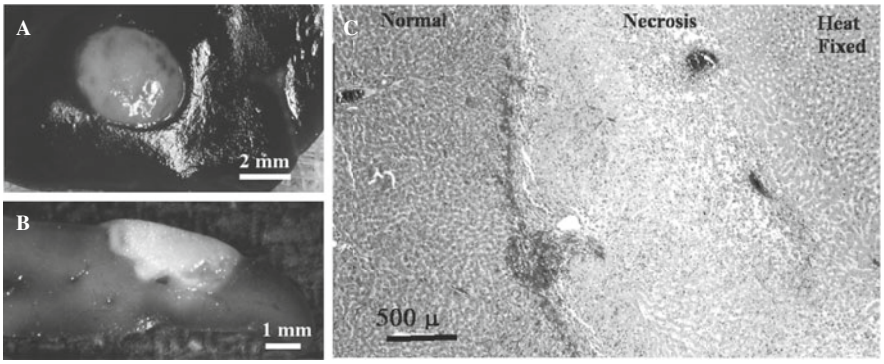

Fig. 13.3 Necrosis of photothermal coagulation lesion in rat liver surviving 3 days after irradiation (cw NdYAG laser; $\lambda = 1.064$ μ; beam spot size, 2 mm; 9 W, 10 s). (**a**) Necrotic lesion, irradiated surface, gross appearance of fresh specimen: the boundary of the opaque, lightly colored necrotic photothermal lesion with the surrounding dark viable liver tissue is very distinct. (**b**) Necrotic lesion, cut surface 10% buffered formalin-fixed gross specimen: the peripheral vascular thermal damage zone is no longer apparent since all damaged cells and tissue in that zone have died and undergone necrosis. (**c**) Necrotic lesion, microscopic appearance: the higher magnification offered by microscopy allows the observation of different types of tissue damage within the necrotic photothermal lesion. The viable, normal liver (*left*) is separated from the dead, necrotic liver (*right*) by a thin band of hemorrhage not visible in the gross specimen. The zone of necrosis includes regions of post-mortem lytic necrosis and post-morterm coagulative necrosis. [H and E stains.]

13.2.3 Mechanisms of Thermal Injury

13.2.3.1 Primary (Direct) Thermal Injury

The mechanisms of primary direct thermal injury of cells and tissues involve the numerous processes of tissue ablation, carbonization, water vaporization, thermal denaturation of proteins and cell membrane rupture (see Table 13.3). The first three mechanisms are very complicated physiochemical reactions that are not explained by simple first-order kinetics. On the other hand, heat-induced intracellular and extracellular protein molecular denaturation and cellular lipoprotein membrane dissociation "melting" and disruption are primary processes that have been shown to be first-order kinetic processes that can be described by the Arrhenius equation as will be discussed in Section 13.3.

Table 13.3 Treatment effects produced along heat gradients extending from hot center of single volume heat source to cooler periphery in vivo and in vitro heating

Treatment effect	Mechanism of treatment effect	Pathologic marker of treatment effect
Tissue ablation	Removal of tissue mass by explosive fragmentation, tissue vaporization and combustion	Defect or hole in tissue
Tissue carbonization	Thermal reduction of organic tissue components to carbon	Thin line of carbon lining ablation defect
Tissue desiccation and vacuolization	Tissue water vaporization and expansion of steam vacuoles entrapped in tissue	Damage zone of vacuolated, shrunken, brittle tissue beneath carbon layer
Thermal tissue coagulation	Thermal denaturation of extracellular matrix proteins Thermal denaturation of cytoskeletal and cell proteins Thermal denaturation of other cellular and tissue proteins	Heat fixation of cells and tissues Loss of native birefringence of collagen, elastin and muscle Hyalinization of collagen Spindling of epithelial cells
Rupture of cellular membranes	Thermal denaturation of vital respiratory enzymes Molecular dissociation of cell Membranes and collapse of cell organelles	Hyperchromasia and spindling of cell nuclei Hyperchromasia of cell cytoplasm

13.2.3.2 Tissue Mass Ablation

For the purposes of this chapter, *tissue* ablation is defined as removal of tissue mass to create a space within the tissue. *Functional* ablation is the removal or modification of a tissue function due to actual removal of mass or lethal injury of tissue. "Ablation" as used in the cardiac clinical literature usually means *functional* ablation. For example, creation of a thermal coagulation lesion in heart muscle is done to "remove" a functional source of cardiac arrhythmias. The *treatment endpoint* is the "ablation" or disappearance of the arrhythmia as monitored by an electrocardiogram and the *pathologic endpoint* is a volume of thermally coagulated (dead) myocardium.

Lists of the mechanisms of laser-mediated tissue ablation can be arranged by temperature gradients beginning at high temperature mechanisms requiring huge amounts of heat energy delivered in very short pulses then proceeding to those associated with lower temperatures and longer irradiation times. These are (1) plasma formation, the ionization of molecules at the irradiated surface; (2) tissue vaporization, the phase changes of solid, organic tissue components to liquids and gases; (3) combustion, rapid oxidation of organic tissue components with production of flames and smoke comprised of various gases and very small carbonized particles

and inorganic ashes; and (4) explosive tissue fragmentation due to rapid expansion and rupture of water vapor (steam) vacuoles in the heated tissues ("popcorn" effect).

Pathologic evaluation of *tissue ablation* involves observation and measurement of what is *not* there, that is, a hole or defect in the tissue at the irradiation site. Also, the defect has to be associated causally with a reasonable thermal history and/or surrounded by other tissue abnormalities that are characteristic of thermal damage and tissue ablation. Otherwise, the naïve (and not-so-naïve) observer could misidentify any old tissue defect as being the "laser photothermal cut" (S. Thomsen and J. Coad, personal experiences, 1979–2008). With proper orientation, measurements of the maximum dimensions the tissue defect and the surrounding zones of thermal tissue damage in the tissue can be done using gross and microscopic observations [19].

13.2.3.3 Carbon Formation and Carmelization of Tissue

Carbon formation is the heat-mediated reduction of tissue and cellular organic molecules to elemental carbon that forms a very thin black membrane (5–20 microns) covering the walls of the defect or the irradiated surface of the tissue (see Figs. 13.2 and 13.4). The clumped black carbon particles are easily seen and measured in properly stained microscopic tissue sections. Carmelization is the melting, partial reduction and resolidification of tissue sugars. It occurs at slightly lower temperatures than carbonization but, in light microscopic histological sections, is frequently overshadowed by carbonization and staining artifacts induced by tissue desiccation. Carbonization is typically associated with local temperatures in excess of 200°C.

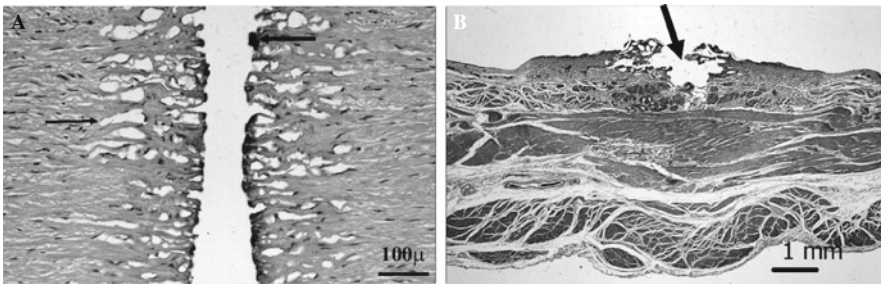

Fig. 13.4 Water vaporization mechanisms: tissue dessication, water vapor vacuole formation and explosive fragmentation. (**a**) Thermal damage zones: carbon formation, caramelization, water vacuole formation and tissue dessication in argon laser irradiated dog aorta. The ablation hole was formed by high energy mechanisms indicated by black carbon granule formation (*thick arrow*) and caramelization of surface tissues and the even sides of the ablation hole. A uniform band of water vapor vacuoles (*thin arrow*) has formed in the hyperchromatic, hyalinized, dessicated, thermally denatured cells and connective tissue located just below the ablation surface. The boundaries of this water vapor vacuolization zone are measurable and can be predicted in rate process mathematical models. (H and E stains. Orig. Mag. 400×) (**b**) Thermal tissue ablation by explosive fragmentation in dog urinary bladder mucosa: argon laser irradiation in vivo. The very irregular ablation defect (*arrow*) was produced by rapid expansion and rupture of large and small, thin-walled water vapor vacuoles. The thin vacuolar walls consisted of desiccated, brittle, thermally denatured tissues. The boundaries of the more peripheral thermal damage zones are not easily recognized at this low magnification. (H and E stains. Orig. Mag. 6.25×.)

13.2.3.4 Water Vaporization

Water vaporization, vapor diffusion and tissue desiccation appear as the tissue temperatures approaches 100°C at standard pressure (Fig. 13.4). When generation of water vapor is faster than its rate of diffusion out of the tissue, the vapor can be trapped within the tissue, forming steam vacuoles. If the incident laser irradiation energy continues to be converted to heat energy, pressure rapidly increases, the steam expands within the vacuoles stretching their now desiccated, brittle, thin walls until they rupture either creating bigger vacuoles below the surface or explosions throwing tissue fragments of the vacuole wall from the surface ("popcorn effect") [20, 24–26].

The temperature history of the "popcorn effect" and explosive vacuole rupture at the tissue surface can be followed using a calibrated thermal camera and a microphone (or ears of the investigators). As irradiation is delivered into the tissues, the surface temperature rises (sometimes up to 130–160°C), the water vapor expands within the vacuoles until they rupture with a loud "pop." The "pop" marks the rapid escape of the steam into the atmosphere and a marked temperature drop to around 100°C, the temperature of water vapor in the remaining tissues. Depending on the tissue temperatures, tissue water content and heating times, a band-like zone of variably sized, intact and ruptured vacuoles can be seen just below the carbon layer in histologic sections [27]. This zone tends to have distinct and measurable borders with the adjacent thermally coagulated (denatured) tissues when viewed with a light microscope and represents a major zone of water-mediated thermal effects in tissues (Fig. 13.4). Although water vaporization is a complicated thermodynamic process, the pathological effects of tissue vacuole formation, expansion, vacuole size and tissue desiccation can be modeled and incorporated into mathematical models of thermal damage in biological tissues [28].

13.2.3.5 Thermal Protein Denaturation (Thermal Protein Coagulation)

General Comments About Tissue Proteins

Proteins are ubiquitous tissue components that include a myriad of pure proteins, lipoproteins and glycoproteins. These molecules form solids, gels, membranes and dissolved materials within (intracellular) and outside (extracellular) the cells that comprise any tissue [15–18, 29, 30]. Cellular enzymes are proteins that act as catalysts needed for proper, coordinated cell functions required for life. They are critical components of systems responsible for (1) energy production, (2) protein, carbohydrate, lipid and DNA/RNA synthesis and degradation, (3) cell repair, (4) transport of nutrients, water, salts, metabolic wastes and secretory products across cell membranes and (5) signal transduction across membranes inside and outside cells.

Proteins also form the important structural components within the cell which are the intracellular cytoplasmic and nuclear skeletal proteins and the cell motility proteins [17, 31, 32]. The intracellular structural and motility proteins are necessary for (1) organelle and cell support, (2) intracellular and transmembrane material transport, (3) cellular movement and (4) reproduction and regeneration with formation of the mitotic spindle for chromosome sorting and movement and the mechanisms for cell division.

The extracellular structural proteins form intricate scaffolding networks and environments necessary for integration of cells into tissues and for coordinated structural and functional organization of tissues to form organs and the whole organism. The most prevalent extracellular structural proteins are (1) the formed elements, collagens, elastins, fibronectin and neutral, basic and acidic aminoglycans and (2) the various amorphous proteins, aminoglycans and polypetides including mucins, globular carrier proteins, and other cell secretions and products. These elements are mixed with water, salts, sugars and polypeptides to form the semi solid gel in which cells reside, function and travel [15, 16, 18, 33–36].

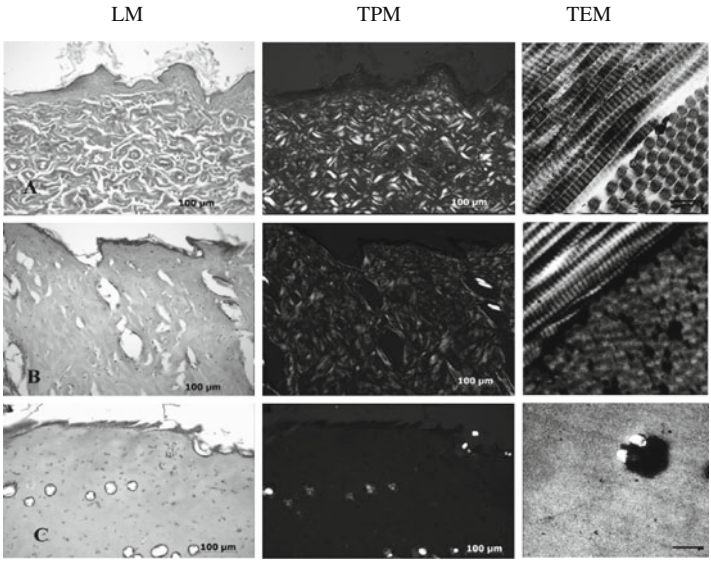

Fig. 13.5 Loss of Type I collagen birefringence image intensity: rat skin heated in vitro in water bath for 20 min at various temperatures. [*Left photos*: H and E stained. Light Microscopic images (LM); center photos: H and E stained. Transmission Polarized Microscopic images (TPM) Orig. Mag. 100×. *Right photos*: Lead citrate and uranyl acetate stains Transmission Electron Microscopic images (TEM). Bar = 200 nm)] (**a**) (*top row*) Rat skin at room temperature: Large concentration of native state relative to concentration of non-native state. The Type I collagen of the skin dermis retains its distinct fibrous pattern and bright birefringence image as seen in the LM and TPM images. The characteristic, semi-crystalline striated arrangement of the collagen molecules forming the collagen fibril demonstrated in this TEM image is responsible for Type I collagen birefringence, the optical property of rotating transmitted polarized light in a dark field. (**b**) (*middle row*) Rat skin heated to 60°C: Decreased concentration of native state relative to concentration of non-native state. The dermal collagen is hyalinized ("glassy") when viewed with LM. However, the residual fibrous pattern is revealed in the TPM of the heated collagen which has undergone a partial loss of birefringence image intensity. TEM shows that collagen fibrils retain their regular longitudinal molecular arrays (striations) responsible for the residual birefringence image. However, the fibrils have swollen, their distinct borders are obscured and are surrounded by darkly stained electron-dense partially denatured proteins and glycoproteins thus producing the homogeneous image of hyalinization in the LM. (**c**) (*bottom row*) Rat skin heated to 90°C: Low – essentially zero – concentration of native state relative to concentration of non-native state. The dermal collagen is now totally homogeneous and the birefringence image is totally lost. TEM shows only finely distributed granules of thermally denatured collagen and considerally larger grains of contaminating dirt

13.2.3.6 Thermal Denaturation of Proteins

The direct, primary thermal effect on the intracellular and extracellular proteins, glycoproteins and lipoproteins of cells and tissues is thermal denaturation of these macromolecules [37–40]. Thermal denaturation is the accumulated structural and functional change in heated protein that result from the physical and chemical molecular disequilibrium and phase changes introduced initially by heating and subsequent cooling. Usually, thermally denaturized macromolecules lose their characteristic quaternary, tertiary and secondary molecular configurations due to disruptions of hydrogen and ionic bonds as well as sulfide and other covalent bonds formed among primary amino acids chains, the building blocks of proteins. In the denaturation process, the molecules are reduced from highly organized, characteristic structures with specific functions to amorphous granules of collapsed and ruptured primary chains with no biological function (see Fig. 13.5). Accumulation of these highly scattering granules is responsible for the generation of the usually opaque, firm white or light tan volumes observed in heated target tissues. The transformation of fried egg whites from clear, viscous fluid rich with the protein, albumin, to a white, opaque solid is the classic example of thermal denaturization of protein [40]. The same denaturation processes are responsible for the loss of native birefringence of Type I collagen and the motor proteins, actin and myosin, in the sarcomeres of skeletal and smooth muscle cells, as discussed in Section 13.3 [41–48].

On the other hand, molecular protein denaturation and dehydration can be associated with transparent clearing of highly scattering, opaque white collagen-rich (Type I collagen) tissues such as skin dermis or muscle tendon [49]. Unfortunately, the temperatures/time at temperature thresholds of thermal clearing are much higher than those associated with cell killing; therefore heat cannot be used to "make skin transparent" since second and third degree burns would be produced.

13.2.3.7 Heating of Cellular Membranes

Cells are membrane-bound bags of proteins, carbohydrates, lipids, water and salts in which are suspended smaller, membrane-bound organelles such as nuclei, endoplasmic reticulum, mitochondria, the Golgi apparatus, secretory vacuoles and phagosomes [15–18, 32, 50]. The organelles compartmentalize, organize and separate different cellular metabolic functions, including energy generation (mitochondria), synthesis of DNA and mRNA (nuclei) and proteins (endoplasmic reticulum), packaging (Golgi apparatus) and storage of secretory products (secretory vacuoles) and degradation products (secondary lysosomes).

Cell membranes are composed of phospholipids oriented into a polar bilayer so that the hypdrophobic portions (fatty acid chains) of the molecule form the inner layers of the membrane and the hydrophilic portions (phosphate or organic esters) form the outer layers to face the watery environments of the extracellular and intracellular spaces. Embedded within and on both surfaces of the cellular membranes are important protein and glycoprotein structures including specific receptor proteins,

water pores, ion channels and enzymes. These proteins are important for transport of nutrients, metabolites, salts and water and signal transduction (stimulating and inhibiting) across the membranes.

When heated above physiological temperatures, the hydrogen bonds between the hydrophobic lipids become weaker and the individual phosholipid molecules separate creating defects in the membranes. The water and solutes within and outside the membrane barriers can leak in and out thus disrupting the intracellular and extracellular functional equilibria of cells and the surrounding the environments. If the heating continues and/or the temperatures increase, the defects enlarge, overwhelming the usual repair mechanisms, and the cell dies.

13.2.4 Mechanisms of Heat-Induced Cell Death

13.2.4.1 "Heat Sensitive" and "Heat Resistant" Cells and Tissues

Thermal denaturation of intracellular and extracellular proteins and molecular dissociation (melting) of cellular membrane lipids result in changes of molecular structure and loss of cellular function that, if sufficiently severe and/or prolonged, will produce lethal thermal damage and cell death. The tissue temperatures and times at temperature at which these changes occur differ among proteins, lipoproteins, glycoproteins, cell membranes and tissues. Some tissue components are more sensitive to heat elevation than others and denature or dissociate at lower temperatures, thus are considered relatively "heat sensitive." Those proteins, glycoproteins and lipoproteins that denature at higher temperatures are considered "heat resistant." A very general order of the range of more heat sensitive to the more heat resistant tissue proteins would be the following: (1) respiratory, energy-generating enzymes of the mitochondria, followed by the (2) intra- and extra-cellular non-structural tissue proteins, glycoproteins and lipoproteins, and lastly, the (3) intra- and extracellular structural tissue proteins. Cell membranes dissociate at low temperatures; therefore, the lipoprotein membranes are more heat sensitive than other cellular proteins [50–52].

13.2.4.2 Minimal Thermal Injury that Leads to Cell Death

To produce the high-energy molecule, adenosine triphosphate (ATP), the respiratory enzymes have to be arranged in a specific order on the inner membrane of the mitochondrion [7, 16, 17]. Therefore, the critical minimal lethal thermal injury to a cell is the rupture and fragmentation of the mitochondrial membrane along with the thermal denaturation of the respiratory enzymes sufficient to produce cell death. However, if the resultant membrane defects are small, they can be repaired and, if few enzymes are denatured, they can be replaced on the membrane by synthesis of new ones. Thus, if sufficiently small, a thermal injury can be considered to be reversible and the cell will survive the injury.

Cell death produced by lethal thermal injury can be due to (1) abrupt physical disruption of cell structure and function and structure by "heat fixation" of proteins in situ, a primary thermal effect, (2) gradual loss of vital cellular functions including disruption and loss of energy production, gradual loss of repair enzyme function and gradual loss of membrane integrity and function, and (3) induction of apoptosis as discussed below. The damage involving gradual loss of vital cellular functions produces severely injured (moribund) cells that can continue to have regions of cytoplasm and nucleoplasm that function for a while, but not at full capacity. These injuries will eventually lead to cellular system failure and death. Therefore, some tests for viability such as cellular dye exclusion and vital stains that rely on the oxidation/reductions functions of certain mitochondrial respiratory enzymes can indicate false "viability" for a time in injured and dying cells. The enzymes may be working for the time being, but the cells and tissues are moribund and eventually will die. Depending on the tissue, organ and animal species, cell and tissue death will occur immediately or within hours, but may take a day or two to become fully manifest by the development of post-mortem necrosis.

The events of isolated cell death by pure apoptotic mechanisms do not lead to post-mortem necrosis [6]. However, in real life and death situations, both post-mortem necrosis and apoptosis can occur in the same tissues and, indeed, may share similar triggering mechanisms [7, 53–56].

The exact temperature/time thresholds for cell death have to be determined for each cell and tissue type. However, some cells are more heat sensitive than others. In general, cancer cells are killed more easily than their normal counterparts. The basic theory of clinical low temperature hyperthermic cancer treatments exploit this temperature/time differential to kill off the cancer cells while sparing the normal ones [57, 58].

13.2.4.3 Post-Mortem Necrosis

Necrosis, by definition, occurs after cell (and tissue) death and involves the degeneration and disintegration of cells and tissues after death [6]. In laymen's terms, necrotic tissues and organs are "rotten" tissues and organs. There are generally two histopathologic types of post-mortem necrosis: lytic necrosis and coagulative necrosis; and, frequently, they are intermixed in the same dead tissue. *Lytic necrosis*, the chemical fragmentation (lysis) of cells, cellular membranes and organelles and extracellular matrix, is due to the extensive and overwhelming effects of proteolytic and lipolytic enzymes [6, 59]. These are enzymes that have either leaked from the ruptured lysosomes of the dead or dying cells themselves or have been secreted by infiltrating inflammatory cells (polymorphonuclear cells). The second type of post-mortem necrosis is *coagulative necrosis*, the gradual degeneration and collapse of cells and cellular organelles [6]. This necrosis is usually associated with loss of energy production by direct mitochondrial dysfunction or by lack of oxygen delivery to the tissue by blocked blood flow (ischemia). Usually, coagulative necrosis occurs in cells that contain relatively few lysosomes and relatively large numbers of mitochondria such as striated muscle cells of the heart and muscloskeletal system. The two types of post-mortem necrosis occur within thermal lesions with the zone of

lytic necrosis being more peripheral to the zone of coagulative post-mortem necrosis since the more peripheral zones receive the infiltrating inflammatory cells with their lytic enzymes first [10, 23] (see Fig. 13.6).

Coagulative post-mortem necrosis is associated with the loss of energy production. The major source of metabolic energy generation occurs in the mitochondria where high energy phosphate bonds of adenosine triphosphate (ATP) are created by chemical reactions catalyzed by the respiratory enzymes. These protein enzymes are found on the inside surface of the folded inner membrane of the mitochondrion arranged in a regular sequential order that allows the efficient functioning of the chain oxidative/reduction reactions that produce ATP [6, 53–56]. Heat-induced mitochondrial membrane rupture will disrupt this highly efficient order and, along with the thermal denaturation of the respiratory enzymes, will lead to insufficient energy production and cell death to be followed by necrosis. However, loss of oxygen due to stoppage of blood flow in the red thermal damage zone can also

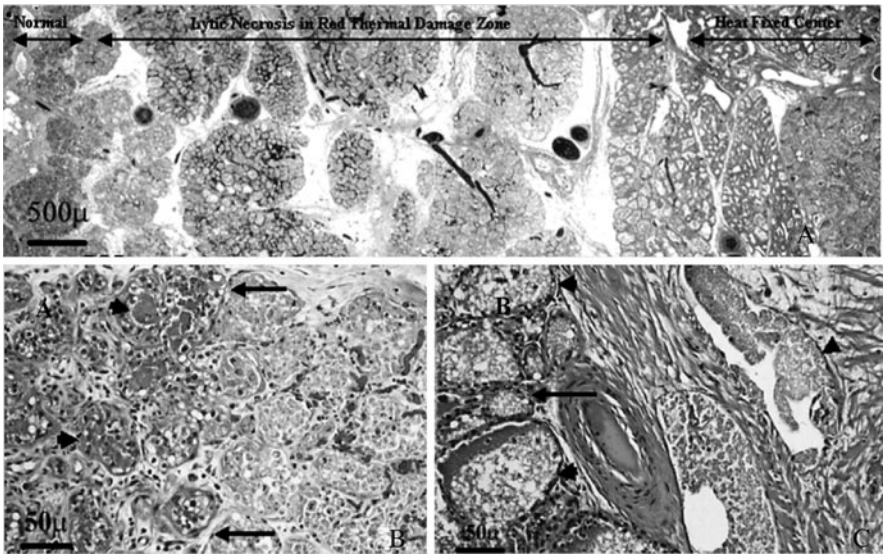

Fig. 13.6 Host responses to lethal thermal damage in post-lactational pig breast at three days survival. (**a**) Microscopic overview of thermal damage zones in pig breast. The boundary between the normal tissue and tissue undergoing lytic necrosis marks the full extent of the thermal treatment effect. This boundary is essentially coincident with the outer boundary of the vascular changes seen in the red thermal damage zone of the acute lesion. (H and E stains. Orig. Mag. 60×) (**b**) Boundary of normal post-lactational breast tissue and lytic necrosis. The boundary (*arrows*) between the viable and necrotic breast tissue is distinct. The viable tissue (left of boundary) consists of glands is composed of the degenerating vacuolated epithelial cells and residual milk proteins in the duct lumens (*arrow heads*) characteristic of the normal physiologic involutional changes in breast after weaning. The necrotic cells of the tissues to the right of the boundary are fragmented and many have no nuclei. H and E stains. Orig. Mag. 640×) (**c**) Heat fixed breast tissue in center of lesion. The hyperchromatic, shrunken nuclei and cytoplasm (*arrows*) are characteristic of thermally denatured (heat fixed) glandular cells. The lumens of the dilated glands are filled with foamy material (*arrow heads*) characteristic of milk production that was thermally fixed in place at the time of treatment three days before. (H and E stains. Orig. Mag. 640×)

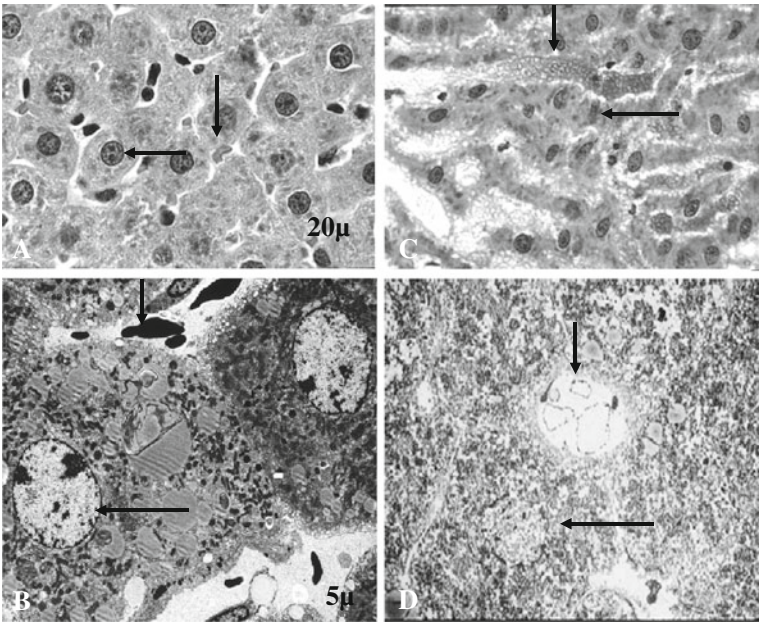

Fig. 13.7 Heat fixation in cw NdYAG (0.9 W, 6 s) laser irradiated rat liver: acute thermal coagulation lesion. (**a** and **b**) Normal liver: the liver cells (*horizontal arrow*) contain sharply demarcated nuclei and distinct cytoplasmic granular structures. The plasma membranes of the red blood cells (*vertical arrows*) are intact. ((**a**) LM H and E stains. Orig Mag. 640×; (**b**) TEM Orig. Mag. 5000×) (**c** and **d**) Heat fixation: in the LM image (**c**), the heat fixed liver cells and their nuclei are shrunken and dark (*horizontal arrow*) with fairly distinct boundaries. But in the TEM image (**d**), the nuclei are obscured (*horizontal arrow*). The thermally denatured nucleoproteins have entrapped the DNA that still binds with the hematoxylin stain in the LM but does not bind the heavy metal salt stains in the TEM. The TEM image shows the empty ghosts of the red blood cells outlined by their ruptured membranes (*vertical arrow*). ((**c**) LM H and E stains. Orig. Mag. 640×. (**d**) TEM Org. Mag. 5000×)

be an important factor in the generation of coagulative post-mortem necrosis due to ishchemia.

13.2.4.4 Cell Death Due to Rapid Thermal Coagulation (Heat Fixation)

Rapid elevations of tissue temperature in a short time can produce sudden death by immediate thermal coagulation and precipitation of cellular and extracellular proteins in situ ("heat fixation"). Concomitant extensive membrane rupture leads to immediate membrane depolarization and leakage of water, salts and small molecules out of the cells and their organelles, but their denatured protein contents stay in place. After this catastrophic death, none of the cells are alive, none of their intrinsic enzymes are functional and the heat fixed cells and extracellular matrix will not undergo post-mortem necrosis. Heat fixed tissues are found in the hottest portion

of the thermal lesion which usually is the center of the lesion. Because heat fixed tissues resemble "living tissues" in routinely-prepared and stained histopathologic sections viewed with a light microscope, numerous investigators (including some pathologists not aware of this phenomenon) have mistakenly reported the centers of thermal lesions as "alive" (see Figs. 13.6 and 13.7).

Eventually, small volumes of heat fixed dead tissue will be liquefied, organized and removed by inflammatory cells directly invading from viable tissue found at the periphery of the thermal lesion or from blood flowing in open lumens of necrotic blood vessels or in new blood vessels formed in wound granulation tissue. However, if the heat fixed volume is sufficiently large and communication cannot be established with the surrounding viable tissue, the heat fixed tissues will slowly fade away into granules, lose water and frequently will undergo calcification (dystrophic calcification) forming a hard mass surrounded by fibrous scar tissue [10].

13.2.4.5 Heat Fixation Vs. Pathophysiologic Post-Mortem Coagulation Necrosis: A Diagnostic Conundrum

In photothermal lesions, coagulative post mortem necrosis is to be distinguished from heat fixation which is the immediate (ms to s) result of direct thermal denaturation (thermal coagulation) and fixation of tissue proteins, glycoproteins and lipoproteins in situ. Heat fixed tissues tend to be in the hottest center of the thermal lesion while the post-mortem coagulative necrosis zone is more peripheral [10, 60]. Heat fixed tissues retain patterns of their cellular structures longer than tissues undergoing post mortem necrosis. Heat fixed cells retain distinct differential staining of the cytoplasmic proteins and nuclear DNA for days to weeks while in most cases of post mortem coagulative necrosis, the nuclear DNA disintegrates and disappears within a week. Ultimately, small volumes of heat fixed tissues will undergo lytic necrosis and organization by inflammatory cells invading from the peripheral viable tissues. However, large volumes of heat fixed tissues in some organs will never be penetrated by inflammatory cells or blood vessels and will never undergo lysis or organization. These volumes will be isolated by scar tissue and persist for several months to years [10].

13.2.4.6 Programmed Cell Death (Apoptosis)

The most critical eukaryotic cell organelles in terms of cell life and death are the mitochondria, intracytoplasmic organelles bound by two membranes that are considered to be the main arbiters of cell life and death [7–9, 53–55, 61]. Mitochondria are not only the sites of the energy production required to sustain life but also they contain the receptors and reactants required for apoptosis. Apoptosis is a physiologic mechanism of cell death in which a series of signal transductions at the mitochondrial or cell membranes initiate an activation cascade of specific mitochondrial and cytoplasmic proteins. These proteins or their precursors have to be in place ready to trigger the energy-requiring chemical reactions that produce characteristic cellular

morphologic and functional alterations over time (hours to 2–3 days) that terminate in fragmentation of the cells with the formation of apoptotic bodies, small bits of cell cytoplasm and nucleus. These apoptotic bodies disappear within a few hours after their formation by being ingested (by phagocytosis) into adjacent living cells where the bodies are digested within secondary lysosomes. Theoretically, no cellular contents are released from the cells dying by apoptosis; therefore there are no cytokines released to promote cellular or vascular inflammatory responses by the host. Some cells are genetically programmed to undergo apoptosis more readily than others. These include endothelial cells, lymphocytes, cells of embryologic tissues and some neoplastic cells. To make things even more confusing, the signals that initiate apoptosis can also activate mechanisms of cell death followed by necrosis. Most thermal lesions contain morphological and chemical markers of both death processes.

13.2.5 Wound Healing

Now that the different mechanisms of cell death and tissue necrosis have been discussed, the next steps the host will initiate will be the resolution of the pathologic effects of the injury, that is, the processes and events of wound healing. These include the activation of the mechanisms of wound healing including (1) organization (2) tissue regeneration, (3) repair and (4) scar tissue formation [6, 62–65].

13.2.5.1 Organization

Inflammatory cells enter the necrotic volumes upon the resumption of blood flow in damaged yet still open blood vessels or by migration from the surrounding viable tissues beginning about 8–12 h after cell and tissue death. Certain inflammatory cells, the macrophages, function as garbage collectors to clean up (organize) the necrotic debris in preparation for the later stages of wound healing: tissue regeneration, repair and scar formation. Depending on the species, organ and tissue, the organization will begin at about 2–7 days after injury. The debris-collecting macrophages phagocytose (“ingest”) the necrotic debris and carry it around in their cytoplasm in specialized intracellular membrane-bound organelles called secondary lysosomes (phagosomes). The “loaded” macrophages then (1) are incorporated into the wound healing tissues and remain in the local tissues, (2) migrate into the lymphatic vascular channels to land and accumulate in lymph nodes (regional “garbage dumps”), or (3) migrate back into blood vessels to be delivered, metabolized, excreted and/or stored in more distant tissues.

13.2.5.2 Tissue Regeneration and Tissue Repair

Some parenchymal cells and tissues such as liver cells, the epidermis of the skin and the glandular epithelium of gastrointestinal tract and breast among others are

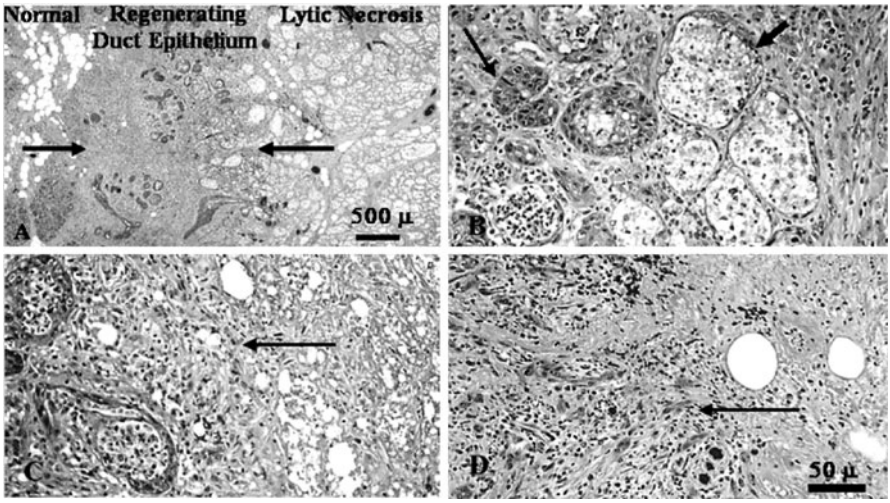

Fig. 13.8 Host responses to lethal thermal damage in pig breast at ten days survival. (**a**) Microscopic overview of healing of thermal lesion. A broad zone of scarring fibrosis and partial epithelial regeneration (*arrows*) separates the now physiologically quiescent, normal fibroglandular-adipose breast tissue from the more central portion of the lesion that is now undergoing lytic necrosis. Although some parenchymal glandular epithelial regeneration has occurred, the functional, lobular glandular pattern has not been reconstituted and the glandular elements are irregularly separated by fibrous scar tissue. (H and E stains. Orig. Mag. 25×) (**b**) Epithelial regeneration into remaining intact glandular connective tissue scaffolding. Regenerating glandular epithelial cells grow along the still-intact basement membrane lining of the breast ducts (*fat short arrow*) to form a lobular gland structure. The epithelium continues to proliferate to fill the duct lumen (*thin long arrow*). The epithelial cells are large with relatively abundant cytoplasm. (H and E stains. Orig. Mag. 640×) (**c**) Epithelial regeneration into region of collapsed necrotic connective tissue. Without the guidance of an intact connective tissue scaffolding, the regenerating epithelial cells grow in a more haphazard pattern. The boundary (*arrow*) between the viable (*left*) and necrotic (*right*) tissue is filled with infiltrating inflammatory cells and proliferating faintly spindled cells that could be activated macrophages, endothelial cells of new blood vessels (vascular granulation tissue) and/or myofibroblasts of new scar tissue (fibrous granulation tissue). (H and E stains. Orig. Mag. 640×) (**d**) Granulation tissue formation at edge of necrotic tissue. The new blood vessels characteristic of early wound healing form irregular, linear structures (*arrow*) in this example of early vascular granulation tissue. No epithelial regeneration is seen in this field. (H and E stains. Orig. Mag. 640×)

capable of regeneration after necrosis (see Fig. 13.8). As long as the usual tissue connective architecture is intact, the regenerating cells will be guided into the connective tissue scaffolding to form normally functional tissue structures such as liver lobules and digestive mucosal glands. The new functional cells are derived from immature, precursor cells in the surrounding viable tissues. These precursor cells are stimulated to proliferate, migrate and mature in response to numerous growth factors produced by the residual, living connective tissue and inflammatory cells at the periphery of the lesion. However, if the necrotic connective tissue scaffolding collapses, the proliferating parenchymal cells pile up into dysfunctional, disorganized

strands or nodules buried in scar tissue. Some adult parenchymal tissues, such as nerve cells of the brain and cardiac muscle cells, do not have readily available, dedicated precursor cells (or very few stem cells that are not easily stimulated to grow and mature) and, in general, are not capable of tissue regeneration. Usually, large volume parenchymal cell regeneration does not occur after large volume necrosis and the tissue repair is mainly by fibrous scar formation to fill in the void.

13.2.5.3 Granulation Tissue and Scar Formation

Whenever a defect is created by the organization of the necrotic tissues, the void is filled with either regenerating tissues or vascular and fibrous granulation tissue (early wound healing tissues) or a mixture of both (see Fig. 13.9). These granulation repair tissues are the earliest forms of scar tissue and will appear in the wound anywhere from 3–5 to 10 days, again, depending on the species and the tissue type within a species. Over the next days to months the scar tissue will be remodeled (regression of the vascular components and thickening of the collagen fibers) and the resultant maturing fibrous scar will contract and become smaller than the original thermal lesion.

13.2.6 Role of Heat Shock Proteins (HSP) in Thermal Lesions

HSP include a group of intracellular proteins that, among many other functions, facilitate the assembly of component peptides into the final configuration of functioning proteins [6, 17, 29, 61]. To initiate heat shock protein synthesis, the cell cultures or tissues are exposed to low temperatures (or other low level injury) for relatively short times. This heating can stimulate specific DNA expression and RNA production for heat shock protein synthesis while not killing the cells by direct injury or by triggering apoptosis. Once the DNA expression/RNA molecules are synthesized, they can remain active for some days so that, if the same cultures or tissues are reheated, the heat shock protein synthetic apparatus is in place and ready to produce new facilitators of enzymatic or structural protein repair. Thus, the cultures/tissues "preconditioned" by the initial heating are more "heat resistant" or protected from thermal injury from subsequent heating episodes because they can institute repair processes more readily than "unconditioned" cultures/tissues.

13.2.7 Mathematical Modeling of Pathophysiologic Thermal Effects

As discussed in great detail in the following Section 13.3, mathematical models estimating pathophysiologic markers (pathologic end points) of thermal damage in cells and tissues that follow first order kinetics can be developed. These can be used

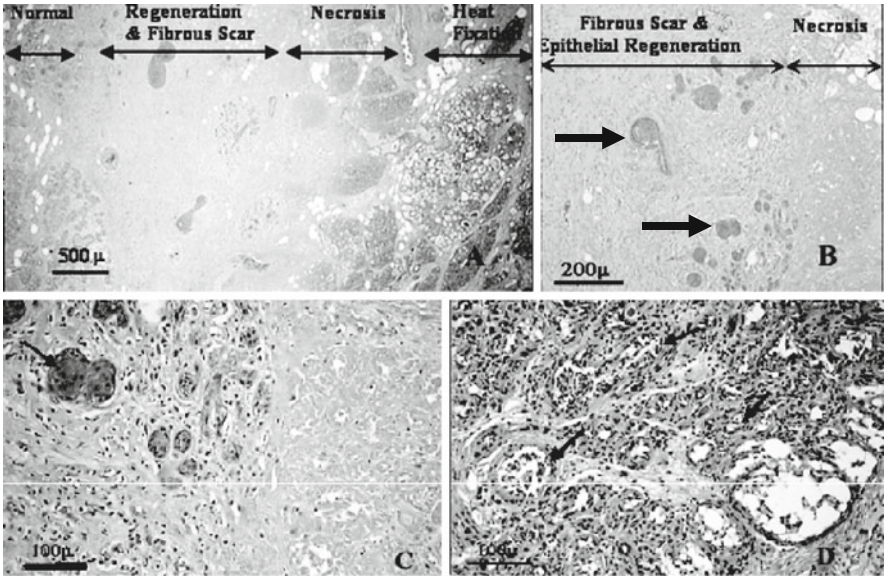

Fig. 13.9 Host responses to lethal thermal damage in pig breast at 28 days survival. (H and E stains) (**a**) Overview of healing thermal lesion. A relatively thick band of fibrous scar tissue that contains a few irregular, variably sized glandular duct structures separates the lobular glandular normal breast tissue from the more central necrotic and heat fixed breast. (Orig. Mag. 6.25×) (**b**) Prominence of fibrous scar tissue formation relative to glandular epithelial regeneration. A higher magnification of the fibrous scar and regenerating glands illustrates the abundance of fibrous scar tissue relative to the paucity of regenerated glandular ducts (*arrows*) in the breast. Fibrous scar tissue formation usually is more dominant relative to regeneration of parenchymal glands in many species. (Orig. Mag. 16×) (**c**) Metaplasia of regenerating glandular epithelium. The regenerating new epithelial cells have changed (metaplasia) from low columnar ductal epithelial cells to larger, more deeply staining stratified squamous epithelial cells (*arrow*). This squamous metaplasia is frequently seen in regenerated tissues of solid glandular structures such as prostate and breast no matter the method of tissue injury is used. The boundary between the viable tissues and necrotic tissues is distinct. (Org. Mag. 500×) (**d**) Persistence of heat fixed tissues. The central heat fixed tissues have disintegrated and shrunken to some extent but still maintain their glandular configuration (*arrows*). No viable cells including infiltrating inflammatory cells have penetrated into the heat fixed tissue volume. (Orig. Mag. 500×)

to describe the temperature/time thermal history, geometry and extent of clinically significant photothermal effects in laser irradiated cells, tissues and organs. Most of these markers or end points are directly related to primary thermal effects such as protein denaturation and cellular membrane rupture ("melting"). They are created at relatively low temperatures (<100°C) but at variable heating times. And, because some of these pathologic markers form distinct lesions with measurable boundaries, they can be described by rate process models whose kinetic coefficients are experimentally derived. Each end point has a unique set of coefficients; therefore, the end points have to be precisely defined to determine the rate coefficients

specific for that particular effect. For example, given equal heating times, the rate coefficients obtained for collagen hyalinization, a protein denaturation process that requires higher temperatures, will be different than the coefficients for cell death due membrane rupture, a lower temperature effect.

13.3 Thermodynamics and Kinetics of Thermal Damage Processes

The thermal aspects of laser-tissue interaction consist of two governing events: (1) the thermodynamics of temperature elevation, and (2) the kinetics of resulting irreversible thermal alterations in tissues. Kinetic and thermodynamic analyses are very different in style in classical treatments. Kinetic analysis concerns the rate at which processes occur; as, for example, reaction rates in chemical transformation of materials. Thermodynamic analysis is usually concerned only with the thermodynamic state change during a process – that is, the rate at which the change takes place is normally not of interest, only the initial and final values of the thermodynamic state variables. There are six thermodynamic state variables, any two of which fully specify the thermodynamic state – i.e. if any two of them are known, the other four may be found uniquely. Consequently, the several state variables comprise a redundant set. Nevertheless, they each provide a somewhat different view of the thermodynamic state, and are thus useful in turn for studying state changes in different ways. The six thermodynamic variables are: temperature, pressure, density, density's inverse specific volume, enthalpy and entropy.

13.3.1 Foundations of Thermal Analysis

The most fundamental of the thermodynamic state variables is temperature; so much so that a whole chapter in this book has been dedicated to its measurement. Two objects are in thermal equilibrium if they are at the same temperature – that is, there will not be a *net* exchange of heat if the objects are placed in contact with each other. Heat is "energy in transit." The so-called "Zeroth Law of Thermodynamics" states that: "if object A is in thermal equilibrium with object B, and object C is also in thermal equilibrium with object B, then object A and object C are in thermal equilibrium with each other."

In the case of laser-tissue interaction, we are interested in the rate of rise of temperature, so the approach in this chapter will be a slightly modified form of thermodynamic analysis: modified to include transient solutions. The thermodynamic processes will be taken to occur under equilibrium or near-equilibrium conditions – that is, state changes occur slowly enough that all thermodynamic variables have the same inter-relationship they would if the rate of change were slowed down even further. Thermal damage kinetics are decidedly non-equilibrium in nature with their rate of change determined by local temperature.

13.3.1.1 Thermal Energy and Enthalpy

Absorption of laser energy results in an increase in the internal thermal energy, U [J] or u [J · kg^{-1}], of the tissue:

$$U = mcT, u = cT \tag{13.1}$$

where m = mass [kg], c = specific heat [J · kg^{-1} · K^{-1}] and T = temperature [K or °C]. This concept is here formulated in terms of a finite "control volume" of material that consists of enough molecules and/or atoms that a spatial and temporal mean value makes sense. Internal thermal energy in this form describes the mean value of the thermal energies of all of the constituent particles in the control volume at the time it is evaluated. Equation (13.1) is not descriptive in a control volume containing only a very few particles that are widely dispersed with an extremely low probability (i.e. rate) of collision with other particles. A statistical (i.e. quantum mechanical) formulation is required to describe those cases. Our case is for aqueous solutions / suspensions, and tissues where the mean time between collisions is vanishingly small; and in the case under study such mean descriptions are extremely useful.

Internal thermal energy is a form of "potential," similar to gravitational potential energy or to electrical potential, so it needs a zero reference point. Thermodynamic tables typically assume zero internal thermal energy at a convenient reference temperature. For example, in the classic "Steam Tables" [66] the reference temperature for the internal thermal energy of liquid phase water is 0°C (273.16 K), and the same reference point for water is used for the enthalpy and the entropy, which remain to be discussed. For most refrigerants (freon, etc.) the reference point is often taken to be −40°C (which just happens to be −40°F as well), the spontaneous freezing point for liquid phase water.

If mass crosses the control volume boundary and/or the pressure or density changes inside the control volume, the total stored (i.e. "available") thermal energy must include "Flow Work" (the pressure-volume product). A more useful description of the available thermal energy is the "enthalpy," H (J) or "specific enthalpy," h [J·kg^{-1}]:

$$H = U + PV;\ h = u + Pv \tag{13.2}$$

where P=pressure [Pa=N · m^{-2}] and V=volume [m^3], v=specific volume [m^3 · kg^{-1}] = $1/\rho$, where ρ = density [kg · m^{-3}]. In studying the units of the equation here, remember that 1 [J] = 1 [N·m]. Enthalpy may properly be thought of as the total thermal energy stored in the volume that is available to do useful work – i.e. it describes the control volume as a thermal engine.

Example 13.1: One gram of incompressible tissue absorbs a total of 2 W for 30 s. If the initial temperature is 37 C, calculate the final temperature after 30 s of absorption. Assume that the effective tissue density is 1050 (kg·m^{-3}) and specific heat is 4050 (J·kg^{-1}). No mass crosses the tissue boundaries in this example.

Solution: All of the energy absorbed goes into raising the temperature – Δv, $\Delta m = 0$:

$$\Delta U\,(\mathrm{J}) = \dot{Q}_{\mathrm{gen}}\left(\mathrm{J}\cdot s^{-1}\right)\Delta t = mc\Delta T$$
$$\Delta U = [2]\,[30] = \left[10^{-3}\right][4050]\,\Delta T$$
$$\Delta T = \frac{60}{4.05} = 14.8\ (^{\circ}\mathrm{C})$$

When mass crosses the volume boundary, it imports thermal energy according to the *net* mass inflow rate, and loses thermal energy proportional to the net mass outflow, or efflux:

$$\frac{\Delta H}{\Delta t} = \frac{\Delta m_{\mathrm{in}}}{\Delta t} c_{\mathrm{in}} T_{\mathrm{in}} - \frac{\Delta m_{\mathrm{out}}}{\Delta t} c_{\mathrm{out}} T \tag{13.3}$$

where m_{in} and m_{out} refer to the mass inflow and outflow, respectively [kg], c_{in} and c_{out} are the respective specific heats [$\mathrm{J\cdot kg^{-1}\cdot K^{-1}}$] and the rate of change in enthalpy is in units of watts [$\mathrm{W = J\cdot s^{-1}}$]. In this formulation we have included only the internal thermal energy contribution, such as would be due to tissue blood perfusion and lymphatic flow. A potential contribution to the total thermal energy, the enthalpy, due to density or pressure change has not been included.

Example 13.2: For the tissue in Example 13.1, assume that a net blood flow of [$0.1\mathrm{g\cdot s^{-1}}$] crosses the boundaries at an inlet temperature of 37°C. Inlet and outlet blood flow are equal in the tissue. Assume that the blood specific heat is the same as water, 4,186 [$\mathrm{J\cdot kg^{-1}}$]. Calculate the tissue temperature at 30 s, as before.

Solution:

(1) We will have to make some assumption about the outlet temperature of the blood. The problem has not been specific about how long the blood remains resident in the tissue. However, the reasonable assumption is that the blood leaves the tissue in thermal equilibrium with it (this is equivalent to assuming that the blood circulation is in "thermally small" vessels).
(2) The temperature rise with no blood flow is substantial, 14.8°C; so, while an accurate solution to this problem requires integrating the transient heat transfer case, we can get a working estimate with a simplified thermodynamic analysis.

$$\Delta U\, mc\,[T - T_0] - \dot{m}_b c_b\,[T - T_0]\,\Delta t = \dot{Q}_{\mathrm{gen}}\Delta t$$
$$\Delta U = [1\times 10^{-3}]\,[4050]\,[T - 37]$$
$$+\,[0.1\times 10^{-3}]\,[4186]\,[T - 37]\,[30] = [2]\,[30]$$
$$\Delta T\,[4.05 + 3.0\times 4.186] = 60\,(\mathrm{J})$$
$$\Delta T = \frac{60}{16.6} = 3.61\ (^{\circ}\mathrm{C})$$

(3) Note the strong effect of the addition of blood flow. (See Fig. 13.2. The regional blood flow was stopped by the initial lesion, the thermal coagulation lesion. Therefore, the adjacent tissue was not cooled during the laser irradiation that resulted in more severe damage, the thermal ablation lesion.)

The effect of heat transfer within the volume is to distribute the internal thermal energy uniformly. Of course, in spatially-distributed laser irradiation patterns, adjacent volumes of tissue will have differing temperatures. Consequently, conduction heat transfer can be a dominant thermal phenomenon, especially in long-term low fluence rate laser activation. Conduction heat transfer is a boundary (surface area) phenomenon:

$$\dot{\boldsymbol{q}}_{\text{cond}} = -k\frac{\partial T}{\partial n} \qquad \dot{\boldsymbol{q}}_{\text{cond}} = -k\nabla T \tag{13.4}$$

where $\dot{q}_{\text{cond}} =$ convection heat flux [W $\cdot$ m^{-2}] in scalar form, k = thermal conductivity [W $\cdot$ m^{-1} $\cdot$ K^{-1}] and n is the normal direction for the surface over which the heat transfer is calculated; $\dot{\boldsymbol{q}}_{\text{cond}}$ is the vector heat flux, and ∇T is the temperature gradient (the gradient of a scalar field is a vector). The negative sign reflects the direction of conduction heat transfer: from higher temperature to lower temperature, i.e. anti-parallel to the temperature gradient (a vector).

Similarly, if there is heat transfer by convection from an exposed control volume surface, it may be found from:

$$\dot{q}_{\text{cond}} = h[T - T_{\text{atm}}] \tag{13.5}$$

where $\dot{q}_{\text{cond}} =$ convection heat flux [W $\cdot$ m^{-2}], h = convection heat transfer coefficient [W $\cdot$ m^{-2} $\cdot$ K^{-1}], and T_{atm} is the atmospheric, or surrounding fluid, temperature [K]. There is also the possibility of thermal radiation from the surface. The direction of convection and radiation heat transfer is normal to the surface ($\boldsymbol{n}$), so the appropriate surface boundary condition is:

$$\mathbf{n} \cdot (k\nabla T) = h[T - T_{\text{atm}}] + \sigma_B\, \varepsilon \left[T^4 - T_{\text{atm}}^4\right] \tag{13.6}$$

where we have now included the contribution of thermal radiation from the surface, as described in Chapter 11 (i.e. σ_B = the Stefan - Boltzmann constant [W $\cdot$ m^{-2} $\cdot$ K^{-4}], and $\varepsilon =$ the surface emissivity, and T is in [K]).

Convection is a special case of conduction heat transfer, where the medium is in motion. Of course, estimation of the convection coefficient becomes quite complex when the fluid near the surface is compressible since the nature of the fluid flow boundary layer (turbulent or laminar) has a very strong influence on the effective convection coefficient. Also, proper formulation of the radiation boundary conditions is even more complex, depending as it does on the shape and coupling factors of surrounding thermal radiation objects, and their temperatures.

Example 13.3: For the tissue under the same conditions as in Example 13.1, assume that the tissue volume is contained in a 1 cm cube. Assume that the tissue volume is at the surface, and has 5 neighbor tissue volumes below and around it. The thermal conductivity is 0.46 [W m^{-1} K^{-1}]. Calculate the net conduction heat transfer out of the tissue volume at the end of the activation (30 s) if the final temperature in the 5 adjacent tissue volumes has risen to half of the temperature in this control volume (i.e. 37 + 14.8 = 51.8°C). Assume that the temperatures represent the values at the centers of the respective control volumes. Neglect inlet and outlet blood flow in the tissue.

Solution:

$$\dot{q}\left(\mathrm{W}\cdot\mathrm{m}^{-2}\right) = k\frac{\Delta T}{\Delta x}$$

(1) Each adjacent control volume (CV) has half the temperature rise of this volume, i.e. 7.4°C. The temperature difference between the adjacent CVs is therefore 7.4°C.
(2) For volumes 1 cm on a side, the distance between adjacent centers is also 1 cm. This means that the temperature gradient is $7.4\,(^{\circ}\mathrm{C}\cdot\mathrm{cm}^{-1}) = 0.074\,(^{\circ}\mathrm{C}\cdot\mathrm{m}^{-1})$.
(3) For the 5 sides the net conduction heat transfer out of the CV is:

$$\dot{Q}\,(\mathrm{W}) = [5]\,[10^{-4}\mathrm{m}^2]\,[0.46]\,[0.074] = 17\,(\mu W)$$

Example 13.4: For the same control volume (CV) as in Example 13.3, calculate the heat transfer by convection from the exposed surface. Assume that $h = 25$ $(\mathrm{W}\cdot\mathrm{m}^{-2}\cdot\mathrm{K}^{-1})$ and the room temperature is 23°C.

Solution:

$$\dot{q}\left(\mathrm{W}\cdot\mathrm{m}^{-2}\right) = h\,[T - T_{\mathrm{atm}}]$$

$$\dot{q}(W) = [1\times 10^{-4}\mathrm{m}^2][25][51/8 - 23^{\circ}\mathrm{C}] = 72(\mathrm{mW})$$

Much more significant than conduction heat transfer.

13.3.1.2 Entropy: The Second Law of Thermodynamics

The energy balance in the first law of thermodynamics (Chapter 10) represents the "break even" thermal point of view. It assumes that all processes are reversible and that all required energy can be accounted for in terms of the thermal energy. That is, there are no "preferred directions" for energy change or for material transformation. It would be equivalent to considering that all chemical reactions are equally likely to occur in either direction. We need some method for identifying preferred pathways

for material transformations, so that we may describe changes that are "more likely," and the concept of "entropy" fills that need.

Classical Thermodynamic Description

As a concept, entropy often gives trouble but it really shouldn't. In perhaps its simplest form, the specific entropy, s ($\mathrm{J{\cdot}kg^{-1}{\cdot}K^{-1}}$), is a measure of randomness or disorder in a system. It is easy to see that a crystalline solid is more ordered than the same substance in liquid or gas phase. As a substance transitions from solid to liquid to gas its entropy increases. It takes energy to create the orderliness of a crystal, so both the enthalpy and the entropy change as a crystal is formed from, say, the liquid phase. Similarly, in chemical reactions the reactants form products because that is more likely than having the products decompose into the reactant atoms or molecules. Hydrogen and oxygen mixtures combine explosively when stimulated to form water; water is an extremely stable molecule that only decomposes to hydrogen and oxygen when considerable energy is added to the system to favor that transition.

Thermodynamic systems (i.e. "heat engines" in the classical sense) are constrained to extract energy from a "thermal energy reservoir" and reject energy to a "thermal energy sink." That is, there will always be "waste heat" for any thermal engine. This is one of the many statements of the "Second Law of Thermodynamics." Others include: (1) the entropy of the universe is always increasing, (2) a perpetual motion machine of the second kind is impossible, and (3) any process that would decrease the entropy of a completely isolated system is impossible (a completely isolated system cannot exchange either heat or mass with the outside world). There are others, as well, but this is enough for illustration. All of them boil down to the simple truth that no thermal system can be 100% efficient.

Heat exchange, for example, is always entropy increasing. When heat, dQ [J], is extracted from a thermal energy reservoir at temperature T_1, the entropy decreases by: $dS_1 = -dQ/T_1$ [$\mathrm{J \cdot K^{-1}}$]. The entropy gained by the extracting object at temperature T_2 is: $dS_2 = +dQ/T_2$. For conduction heat transfer, it must always be true that $T_1 > T_2$, so the net entropy in the universe, $S_u = dS_1 + dS_2$, has increased because of the heat transfer. This leads to the "Clausius Inequality" [67]:

$$\oint_{\Sigma} \frac{dQ}{T} \leq 0 \tag{13.7}$$

Here the closed surface integral is used to denote the *net* entropy change for the *system* (that is, the system must reject heat to the universe in order to function), and Σ is the closed outer boundary of the thermodynamic system.

A single DNA molecule is very well-ordered, and thus at low entropy compared to the constituent molecules required to form it. This might, at first glance, seem to violate the Second Law, but it doesn't because the relative "orderliness" of the unused fractions of the reactants is so much less than their original form

that the randomness in the universe has increased because of the formation of the DNA molecule. The cell is an open system, and the entropy of the byproducts of metabolism is greater than that of the organized molecules created with them, such as DNA, RNA, ATP and, of course, many others. In addition, every biologic cell generates excess heat of metabolic reactions, the waste heat of the cell as a thermal engine, that must be rejected to the environment. All cells obey the Second Law, just as any heat engine must. If a cell is placed in a completely insulated container, it will die as its temperature increases (essentially without bound) in order to satisfy the Second Law.

Perhaps the most pertinent example for this chapter is the change from liquid phase to vapor phase water (boiling) at constant temperature and pressure – this requires the addition of sufficient thermal energy to increase the entropy of the water to that of the vapor phase. At saturation both the pressure and temperature are constant and both the change in enthalpy, $\Delta h\,[\mathrm{J}\cdot\mathrm{kg}^{-1}]$, and the resulting change in entropy, $\Delta s\,[\mathrm{J}\cdot\mathrm{kg}^{-1}\cdot\mathrm{K}^{-1}]$, depend on the temperature at which the boiling takes place:

$$\Delta h = T\Delta s \tag{13.8}$$

In the Steam Tables [66] the somewhat arbitrary reference point for entropy is $s = 0$ at $T = 0°\mathrm{C}$ (273.16 [K]) – this is the triple point for water at pressure $P = 1$ atmosphere (i.e. 101.3 [kPa]). At the triple point, the liquid, vapor and solid phase are in thermal equilibrium, so it makes a convenient reference for both the enthalpy and the entropy of water.

Example 13.5: Calculate the thermal energy ($\Delta h = h_{fg}$) required to boil 10 g of water at 1 atmosphere pressure and saturation temperature (i.e. 100°C) if you know that the change in entropy is $\Delta s = s_{fg} = 6036$ (J/kg/K). Here the "*fg*" subscript indicates the change in phase from fluid to gas. Compare the answer with the tabulated phase change enthalpy at saturation, $h_{fg} = 2.257 \times 10^6$ (J/kg).

Solution:

$\Delta h = T\Delta s = (100+273.16)^*(6036) = 2.252\times 10^6$ (J/kg) . . . within round-off error of h_{fg}
(Note: Don't forget to use absolute temperature here!)
10 g = 0.01 kg => Energy required: $\Delta h = 2.252 \times 10^4$(J)

A similar change in entropy accompanies chemical reactions. The enthalphy change includes Gibb's Free Energy of Formation, $\Delta g\,[\mathrm{J}\cdot\mathrm{kg}^{-1}]$, and the entropy change of the reaction:

$$\Delta h = \Delta g + T\Delta s \tag{13.9}$$

Remember that some reactions are exothermic and others are endothermic as a result of the relative Gibb's energy of formation. We will make use of this relation in a later section of this chapter.

Statistical Thermodynamic Description

Up to this point the discussion of thermodynamics has been limited to the macroscopic (i.e. classical thermodynamics) point of view: quantities such as enthalpy and internal thermal energy are deterministic macroscopic properties and considered continuous. In classical thermodynamics they may be traded between control volumes in infinitessimally small amounts with no lower limit. The classical thermodynamic relationships are routinely used to describe systems as diverse as steam engines, gas turbines, refrigerators, subsonic and supersonic nozzle expansions and living cells.

But entropy is really a stochastic (random) quantity, as described above, and not deterministic (non-random). We should therefore expect a stochastic (microscopic) description, then, in terms of random variables. This point of view was originally proposed by Boltzmann in the middle of the 19th century, and was quite controversial at the time. Very briefly, the entropy is an "extensive" property; that is, it is the sum of the entropies of all of the particles (molecules or atoms) of a system. Further, the permitted "states" of individual particles of matter are not continuous, but are limited to discretely quantized values. This is a fundamental tenet of quantum mechanics. Systems of many interacting molecules undergo continuous change in their quantum state, exchanging energy in numbers of finite, discrete "quanta," and in no smaller amount.

If we follow the thermal energy of an individual molecule for a period of time, we would expect to observe a mean value with discrete (i.e. quantum) fluctuations about the mean described by the various statistical moments: mean, standard deviation, variance, and so on. A very highly ordered ensemble of molecules will have a very small standard deviation, and a more disordered ensemble will have a large standard deviation (looking at just the first and second statistical moments for this discussion). The Quantum State Probability, $p_i(t)$ can be used to describe this, where $p_i =$ the fraction of total molecules in state "i" at any time. If the total number of possible quantum states is low, then the p_i values will be high (and the standard deviation low); and the converse. At all times, the total probability $= 1$, so for N total states:

$$\sum_{i=1}^{N} p_i = 1 \tag{13.10}$$

The macroscopic property used in the previous discussion is the probability-weighted (expected) value, which is called the mean value – for example, the macroscopic internal thermal energy, u, is the mean value, $<u>$, of the allowed quantum state molecular thermal energies, u_i. Note that $<u>$ can be continuous even though u_i is discrete since the mean value of a random process need not be an observable value. If there are N total allowed quantum states, then at any instant:

$$u = \sum_{i=1}^{N} p_i u_i [\mathrm{J} \cdot \mathrm{kg}^{-1}] \tag{13.11}$$

If a complete thermal system, C, contains constituents A and B, where there are N allowed states for A molecules and M allowed states for B molecules, then the complete system, C, is described by their joint probabilities, $p_{ij} = p_i \cdot p_j$. That is, the joint probability is the product of the individual probabilities when the two random processes are statistically independent. To construct a useful model for the entropy of the thermodynamic system, we use the joint probability in the form of an equivalent function, f (as yet undefined):

$$s = \sum_{i=1}^{N}\sum_{j=1}^{M} p_i\, p_j\, f\left(p_i\,,\ p_j\right) = \sum_{i=1}^{N}\sum_{j=1}^{M} p_i\, p_j\, f\left(p_i\ \cdot\ p_j\right) = \sum_{i=1}^{N} p_i f\left(p_i\right) + \sum_{j=1}^{M} p_j f\left(p_j\right) \tag{13.12}$$

The function f must be such that statistical independence – i.e. Eq. (13.12) – holds irrespective of the values of p_i and p_j. One such function that always satisfies this requirement is the natural logarithm, $f(\arg) = \ln(\arg)$ – i.e. $\ln\{AB\} = \ln\{A\} + \ln\{B\}$. It can be shown after some development (see, for example, [68], Chapter 6) that the general solution to the governing second order differential equation is $f = C\ln\{p_i\}$, and since p_i is always ≤ 1, the constant C must be less than zero so that f is positive-definite. Boltzmann demonstrated that the definition of temperature in the statistical and classical domains would be the same if:

$$s = -k\sum_{i=1}^{N} p_i\ \ln\{p_i\}[\mathrm{J}\cdot\mathrm{kg}^{-1}\cdot\mathrm{K}^{-1}] \tag{13.13}$$

where k = Boltzmann's constant$(1.380 \times 10^{-23}\mathrm{J}\cdot\mathrm{K}^{-1})$ and the negative sign is necessary since the quantum state probabilities are constrained to $0 < p_i \leq 1$.

If all of the allowed quantum states are equally likely – that is, if p_i is uniformly distributed – and there are W allowed states, then Boltzmann demonstrated that:

$$s = k\ln\{W\} \tag{13.14}$$

A uniformly distributed random variable is one that maximizes the entropy in a system of molecules. Equation (13.14) is the Boltzmann definition of entropy, while Eq. (13.13) is the Gibbs definition of entropy. When first introduced, Eq. (13.14) was an extremely controversial construction; so much so that Boltzmann was vilified by the thermodynamic classicists of the day. His final word on the matter was to use Eq. (13.14) as his epitaph.

In summary, while the detailed thermodynamic state must be described by quantum mechanical statistical thermodynamics, the mean thermodynamic properties are adequate for laser heating calculations unless the distribution of states deviates significantly from the equilibrium distribution. That is to say, classical thermodynamic variables adequately describe the processes unless all of the events occur in *extremely* short time intervals (i.e. time intervals approaching the mean time between collisions).

The Zeroth Law of Thermodynamics states that "there is a thermal game;" the First Law says that "the best that you can do is to break even," and the Second Law says that "you can never do that well." An unstated Third Law is that "you can *never* get out of the game."

13.3.2 Modeling Tissue Thermal Events

13.3.2.1 Sub-Coagulation Thermal Models

An energy balance for tissue under laser irradiation where metabolic heat and phase change are negligible can be assumed to follow the traditional Bioheat Equation as previously described, and repeated here:

$$\rho c \frac{dT}{dt} = \dot{Q}_{\text{gen}} + \nabla \cdot (k \nabla T) + \dot{w} \rho c_b \, [T_b - T] + \dot{Q}_{\text{met}} [\text{W} \cdot \text{m}^{-3}] \qquad (13.15)$$

where the "b" subscript refers to blood properties, and $\dot{w}$ is the tissue perfusion $[\text{kg}_\text{b} \cdot \text{kg}_\text{tissue}^{-1} \cdot \text{s}^{-1}]$. In Chapter 3, the notation for laser heat generation is S; but since S is used for entropy in this chapter we have used $\dot{Q}$.

13.3.2.2 Evaporation of Surface Water

Surface water evaporation typically dominates other surface loss terms (convection and radiation) above about 60°C [69]. A useful model for evaporation using Stelling's Formula has been derived from experimental solar pond data, as described in [70]:

$$W_{\text{evap}} = [A_s + B_s U_{\text{inf}}] \; (P_{\text{sat}}(T) - E_{\text{atm}}) \, [\text{m} \cdot \text{s}^{-1}] \qquad (13.16)$$

where W_{evap} = surface evaporation rate $[\text{m} \cdot \text{s}^{-1}]$, $A_s = 7.31 \times 10^{-11}$ $[\text{m} \cdot \text{Pa}^{-1} \cdot \text{s}^{-1}]$, $B_s = 1.2 \times 10^{-11}$ $[\text{Pa}^{-1}]$, U_{inf} = free stream air velocity above the surface $[\text{m} \cdot \text{s}^{-1}]$, $P_{\text{sat}}(T)$ = the saturation pressure at tissue temperature, T, [Pa], and E_{atm} = atmospheric water vapor pressure = $(Hu) P_{\text{sat}}(T_{\text{inf}})$ [Pa], where Hu = relative humidity (expressed as a fraction). To include this process in model calculations, the evaporation rate, W_{evap}, is multiplied by the control volume surface area, A $[\text{m}^2]$, liquid-phase density ρ $[\text{kg} \cdot \text{m}^{-3}]$, phase change enthalpy h_{fg} $[\text{J} \cdot \text{kg}^{-1}]$, and divided by the control volume, V $[\text{m}^3]$, to get the equivalent volumetric power, Q_{evap} $[\text{W} \cdot \text{m}^{-3}]$:

$$\dot{Q}_{\text{evap}} = \frac{A h_{fg} \rho W_{\text{evap}}}{V} [\text{W} \cdot \text{m}^{-3}] \qquad (13.17)$$

Here "f" indicates the liquid state, and "g" the gas state, as above.

13.3.2.3 Water Vaporization

When liquid-phase water is vaporized (boiled) we must add the required thermal energy at the boiling point temperature and pressure, T_{sat} and P_{sat}, in the form of the vaporization enthalpy, Δh_{fg}, and as a result the entropy will change, Δs_{fg}, as well as the density (or specific volume). The density/specific volume change is actually included in the phase change enthalpy:

$$\Delta h_{fg} = T\Delta s_{fg} \; = \Delta u_{fg} + P_{\text{sat}}\Delta v_{fg} \tag{13.18}$$

where Δu_{fg} is the internal thermal energy of phase change $= [c_g - c_f]T_{\text{sat}}$, and Δv_{fg} is the change in specific volume at the boiling point pressure, P_{sat}. For example, at 100°C water has (see Example 13.4):

$$\Delta h_{fg} = 2.257 \times 10^6\,[\text{J}\cdot\text{kg}^{-1}],\ \rho_{\text{sat}} = 958\,[\text{kg}\cdot\text{m}^{-3}],\ \Delta s_{fg} = 6036\,[\text{J}\cdot\text{kg}^{-1}\cdot\text{K}^{-1}]$$

Aside from the effect vaporization has on tissue optics, expansion of the tissue water, whether or not phase change takes place, accounts for the internal stresses applied to tissue. In order to include these effects in the energy balance, the left hand side of the energy balance, Eq. (13.15), must be modified. Neglecting perfusion and metabolic heat for the moment:

$$\frac{\partial\,(ph)}{\partial t} \;=\; \dot{Q}_{\text{gen}} \;+\; \nabla\,\cdot\,(k\nabla T) \tag{13.19}$$

The enthalpy is the sum of internal thermal energy and the pressure-volume product, as in Eq. (13.2). Note that the thermal model now includes phase change since the pressure-volume product has been included in the enthalpy.

Numerical implementation of this model may follow the same philosophy as that of the low temperature case if two thermodynamic parameters can be evaluated, $\partial P/\partial T$ and $\partial\rho/\partial T$:

$$\left\{\rho c \;+\; \frac{\partial P}{\partial T} \;-\; \frac{P}{\rho}\,\frac{\partial \rho}{\partial T}\right\}\,\frac{\partial T}{\partial t} \;=\; \dot{Q}_{\text{gen}} \;+\; \nabla\,\cdot\,(k\nabla T) \tag{13.20}$$

In free liquid phase water that is not constrained by rigid or visco-elastic tissue structures, $\partial P/\partial T$ is usually negligibly small. However, a fourth order polynomial fit ($r^2 = 1.000$) derived from "The Thermodynamic Properties of Steam" [66] for the saturation pressure is:

$$\begin{aligned} P_{\text{sat}}\,(T) \;&= 1.686 \times 10^{-9}T^5 \;+\; 6.681 \times 10^{-8}T^4 \\ &\quad +\; 2.411 \times 10^{-4}T^3 \;-\; 0.03623T^2 \;+\; 2.389T \;-\; 0.432 \end{aligned} \tag{13.21}$$

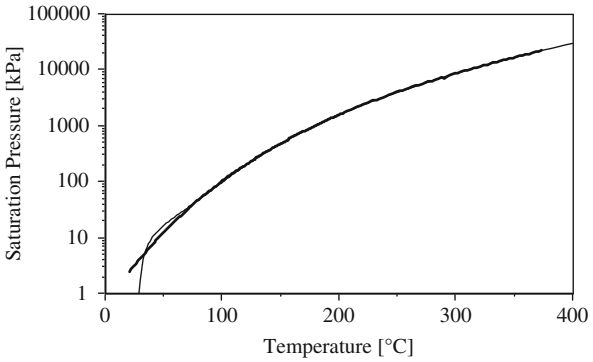

Fig. 13.10 Saturation pressure, P_{sat} [kPa] vs. temperature, T [°C]. *Thick line* plot is experimental data (—), and polynomial fit of Eq. (13.21), *thin line* (—)

where P_{sat} is in [kPa = kN·m^{-2}] and T is in Celsius. In Fig. 13.10 this function deviates from the tabulated data only at temperatures near the freezing point, 0°C. The $\partial P/\partial T$ term may be quickly derived from this polynomial fit.

The density change term cannot be neglected in free water. This additional term (when phase change is included) accounts for the kinetic energy imparted to expelled water and describes the origin of acoustic waves in tissue, whether or not phase change is significant. For no vaporization, an estimate of $\partial\rho/\partial T$ can be obtained from the saturation density vs. temperature curve under the valid assumption that the liquid phase water density is primarily determined by temperature rather than local pressure. The saturation density curve, a fifth order polynomial fit from 20 to 374 C ($r^2 = 0.998$) [66] is:

$$\begin{aligned}\rho_{sat}(T) = &6.918 \times 10^{-10}T^5 + 5.594 \times 10^{-7}T^4 - 1.650 \\ &\times 10^{-4}T^3 + 0.01912T^2 - 1.413T + 1026\end{aligned} \tag{13.22}$$

where ρ_{sat} is in [kg·m^{-3}] and, again, T is in Celsius. In Fig. 13.11 the polynomial fit only deviates significantly from the tabulated data at temperatures near the critical point, 375°C.

At temperatures above about 90°C water behavior dominates the observed photo-thermal phenomena. Below the saturation temperature, 100°C at atmospheric pressure, water vaporization is a diffusion-limited surface loss phenomenon (see Eq. (13.16)) – and depends primarily on surface characteristics such as local humidity and temperature dependent mass diffusion coefficients. Above the saturation temperature, the vaporization process becomes a volumetric energy sink in which phase changes generate high local pressures and concomitant tissue stresses. However, the more moderate heating case is of immediate interest in this discussion.

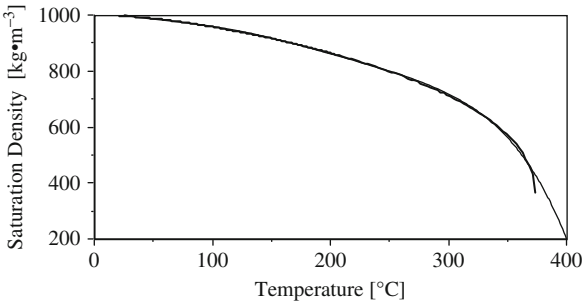

Fig. 13.11 Density of saturated liquid water, ρ_{sat} [kg·m^{-3}], vs. temperature, T [°C]. *Thick line* plot is experimental data (—), and polynomial fit of Eq. (13.22), *thin line* (—)

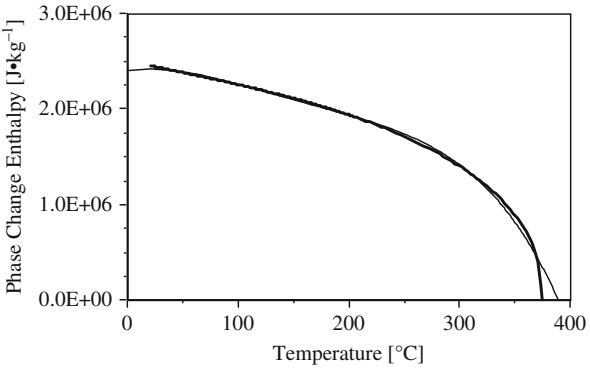

Fig. 13.12 Phase change enthalpy, ρ_{sat}[kg · m^{-3}], vs. temperature, T [°C]. *Thick line* plot is experimental data (—), and polynomial fit of Eq. (13.24), *thin line* (—)

In Fig. 13.10 the saturation pressure at 120°C has increased to 2 atmospheres (200.2 kPa) and climbs precipitously above that. Water vaporization may be included in the modified energy balance of Eq. (13.20):

$$\left\{\rho c + \frac{\partial P}{\partial T} - \frac{P}{\rho}\frac{\partial \rho}{\partial T}\right\}\frac{\partial T}{\partial t} = \dot{Q}_{\text{gen}} + \nabla \cdot (k\nabla T) - \frac{\partial m}{\partial t}\Delta h_{fg}(T) \qquad (13.23)$$

where $\partial m/\partial t$ is the rate of mass vaporization of water per unit volume (kg·s^{-1}·m^{-3}) and $\Delta h_{fg}(T)$ is the temperature dependent phase change enthalpy [J·kg^{-1}] (Fig. 13.12 and Eq. 13.24).

The temperature dependence of saturation density and saturation pressure may be included by incorporating the appropriate correlation relation from Eqs. (13.21) and (13.22). The temperature dependence of the phase change enthalpy may be included using a similar correlation ($r^2 = 0.995$) derived from the same tabular data [66]:

$$\Delta h_{fg} = -4.143 \times 10^{-4} T^4 + 0.247 T^3 - 54.3 T^2 + 1975 T + 2.402 \times 10^6 \quad (13.24)$$

where Δh_{fg} is in [J·kg^{-1}] and T is in Celsius. The polynomial fit only deviates significantly from the tabulated data at temperatures near the critical point.

An alternate, and in some ways equivalent, formulation for vaporization was recently presented by [71] in which phase change processes are included in the left hand side of Eq. (13.15) to obtain an effective specific heat, C', where C' combines the first term on the left hand side with the last term on the right hand side of Eq. (13.23):

$$\rho C' \frac{\partial T}{\partial t} = \rho \left\{ c - \Delta h_{fg} \frac{\partial \rho_w}{\partial T} \right\} \frac{\partial T}{\partial t} = \dot{Q}_{\text{gen}} + \nabla \cdot (k \nabla T) + W \rho_b c_b [T_b - T] \quad (13.25)$$

where W is described in their paper as the "density" of the tissue water, and the perfusion heat has been included. This formulation includes the latent heat of vaporization, but not the changes in tissue density or pressure. However, it has to be used with some caution. First, "W" includes much more than the density of water – in fact, W includes the mass fraction of water in the tissue, so $W = m$ in Eq. (13.23). Second, applying the relation directly as given leads to a decidedly aphysical relationship. That is, for equilibrium vaporization at the saturation temperature $\partial T / \partial t = 0$; consequently, the left hand side of Eq. (13.25) is zero for equilibrium boiling at saturation. The right hand side is certainly not zero – imagine tissue with zero blood flow at uniform temperature (so that both the Fourier conduction term and the blood flow term are zero); $\dot{Q}_{\text{gen}}$ is not zero. The energy balancing effect of the $\partial m / \partial t$ on the right hand side of Eq. (13.23) has been eliminated, leading to an invalid conclusion from Eq. (13.25).

In a numerical model, one may assume that vaporization occurs at local saturation conditions (equilibrium thermodynamics applies) with rate determined by laser excess energy (that is, energy in excess of that consumed by conduction heat transfer, perfusion heat and other losses) and thermodynamic properties. This is equivalent to assuming that evolved water vapor diffuses readily through the tissue structure, and the pressure does not rise significantly. Under these conditions the left hand side of Eq. (13.23) would be zero – i.e. constant temperature boiling at the saturation temperature.

When laser energy, $\dot{Q}_{\text{gen}}$, is added faster than water vapor can diffuse through tissue to maintain liquid saturation at atmospheric pressure, the tissue temperature readily exceeds 100°C when the local tissue pressure rises (and thus lowers the phase change enthalpy). In that case, Eq. (13.23) would have to be used to construct the model. An additional relation would have to be included to complete the model: the rate of pressure rise with water vaporization. The constraints on intracellular water are more significant than on extra-cellular water. That is, extra-cellular expanded water and water vapor need only to "percolate" through spaces in the gross structure while intracellular water vapor expands cell volume putting stress on the cell membrane. For either the intra- or extra-cellular tissue water compartment one would need mass diffusion relations to formulate this term.

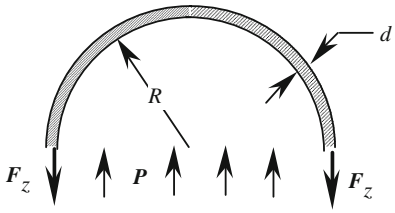

Fig. 13.13 Free-body force diagram of spherical "cell" of radius R with membrane of thickness d stressed by internal pressure, P

The applied stresses, both intra-cellular and extra-cellular, create what can be described as a "thin wall pressure vessel problem." Imagine a spherical pressurized vessel (i.e. cell), such as shown in cross-section in Fig. 13.13, with internal pressure "P" (relative to the external pressure), interior radius "R" and wall thickness, "d." If we cut the spherical vessel at $z = 0$, a free-body diagram reveals that the pressure force, $F_p = \pi R^2 P$, must be balanced by the total Z-direction force, $F_z[N] = 2\pi R d\,\sigma$, where σ [N · m^{-2}] is the wall stress, and so:

$$\sigma = \frac{P\,R}{2d} \tag{13.26}$$

In many cases the local pressure increases cause rupture in the tissue structure, histologically observable as the "popcorn" effect described in Section 13.2.3.4. Elevated tissue pressures also explain the readily observed tearing phenomena in highly layered tissues, such as arterial vessel wall, when irradiated with highly scattered wavelengths. The effects of high local tissue pressures have been observed in many studies when, for example, highly-scattered argon laser irradiation is used to ablate aorta. The scattering events result in high fluence rates just below the tissue surface and corresponding thermally-induced stresses when the tissue water vaporizes.

Example 13.6: This example will adapt "thin wall pressure vessel" analysis to calculate the internal pressure of small bubbles generated in liquid phase water. In this case the "surface tension" or surface free energy, γ(N · m^{-1}) has the role of the "applied stress," σ in Eq. (13.26). The surface tension of water is approximately linearly related to the temperature by γ(dynes · cm^{-1}) = 76.42 − 0.1731 T(°C). Calculate the internal pressure of a water vapor bubble 0.1 mm in diameter in water at 90°C.

Solution:

(1) The pressure forces, F_p, are balanced by the surface tension forces around the circumference of the bubble$_\gamma$, similar to the wall stresses in Fig. 13.13. So:

$$F_p = P\pi R^2 = F_\gamma = \gamma 2\pi R$$

$$P = \frac{2\gamma}{R}\left[\text{N} \cdot \text{m}^{-2}\right]$$

(2) At $T = 90°\text{C}$, $\gamma = 76.4 - 0.1731\,(90) = 60.9\,(\text{dynes} \cdot \text{cm}^{-1}) = 60.8 \times 10^{-7}$ $(\text{N} \cdot \text{m}^{-1})$

$$P = \frac{2[60.8 \times 10^{-7}]}{[0.05 \times 10^{-3}\text{m}]} = 0.243\left(\text{N} \cdot \text{m}^{-2}\right) = 0.243\,(Pa)$$

(3) This is a very small internal pressure.

A model based on the energy balance of Eq. (13.23) should use a small time step so that the contributions of local heat transfer may be calculated and summed with the laser power term. Excess energy above that required to maintain constant temperature may be imagined to go into the vaporization process at the local temperature and pressure. The effect of vaporization on the local pressure may be calculated if an acceptable model for tissue mechanical response is available (i.e. the stress-strain relation, and vapor diffusion coefficients).

At extreme heating rates in tissue and/or free water, such as are realized by pulsed excimer laser activations, the water may become metastable. If so, the vaporization is a rate-limited nucleate boiling phenomenon with rate coefficients determined by the supersaturation ratio, P/P_{sat}, (where P_{sat} is the saturation pressure, Fig. 13.10) and by the surface free energy of nucleated vapor bubbles in the liquid phase. Nucleate boiling only dominates equilibrium boiling at temperatures approaching the critical temperature. In the excimer laser rapid-ablation case the energy powering the debris plume probably comes from nearly instantaneous water phase changes at highly elevated pressures.

13.3.2.4 Coagulation Processes

At higher temperatures the desired thermal end point is coagulation, or a significant irreversible alteration in tissue structural proteins – that is, thermal damage. We often use kinetic models in a "volume fraction" or "probability" form (% of tissue damaged) to predict or describe the evolution of thermal damage. Typical damage processes for which the volume fraction kinetic damage model has been used successfully include: (1) tissue necrosis, (2) loss of birefringence in muscle and collagen, and (3) collagen shrinkage. The damage model is based on the assumption that a single damage process is active, which may not hold in the general case where multiple simultaneous processes occur. Still, the model can be used if the damage processes under study have different basic mechanisms and threshold temperatures and can therefore be considered thermodynamically independent. For example, it is hard to imagine how red blood cell coagulation could affect collagen fiber unraveling, so many common damage processes are quite obviously independent in the thermodynamic sense. In practical calculations, we wish to identify particular damage processes that can act as hallmarks of desired therapeutic end points. As we frequently do not have data for the damage process enthalpy, we

generally do not include the damage process in the thermodynamic calculations of tissue temperature.

Damage processes in tissue coagulation and necrosis typically follow first order unimolecular reaction kinetics. This is such an important topic that it is reserved for detailed discussion in the following section of the chapter, Section 13.3.3. It is very important to note at this point that tissue damage processes are not phase change processes, despite their rather unfortunate previous description in that fashion [37]. It is easy to see why that is so: all phase changes are reversible, all tissue thermal damage processes are irreversible. Repairing tissue thermal damage requires tremendous amounts of energy during the healing (repair and replacement) process.

13.3.3 Kinetics of Thermal Damage Processes

Damage processes can often be modeled as first-order rate processes for which two experimentally derived coefficients are sufficient. Thermal damage in this formulation is exponentially dependent on temperature and linearly dependent on time of exposure. The rate process models apply well to the prediction of damage thresholds, and less well as the damage becomes complete since several of the fundamental assumptions are violated. This section reviews the basis for kinetic models of tissue thermal damage.

13.3.3.1 Theoretical Foundations

The original work on the application of rate process models to thermal damage was reported by Moritz and Henriques in a series of seminal papers entitled "Studies of Thermal Injury" in 1947 [72–75]. In their work, the damage was quantified using a single parameter, Ω, which ranges on the entire positive real axis and is calculated from an Arrhenius integral:

$$\Omega(\tau) = \int_0^{\tau} A\, e^{\left[\frac{-E_a}{R\,T(t)}\right]}\, dt \tag{13.27}$$

where A is a frequency factor [s^{-1}], τ the total heating time (s), E_a an activation energy barrier [$J \cdot mole^{-1}$], R the universal gas constant, 8.3143 [$J \cdot mole^{-1} \cdot K^{-1}$], and T the absolute temperature [K]. One difficulty with this description is that a single damage parameter inherently lumps all damage processes into one global measure, so in multiple damage process cases the lowest temperature process saturates the damage measure early during a laser activation. In this discussion we review the underlying assumptions and origin of the terms in Eq. (13.27) and recast the traditional thermal damage parameter, Ω, into a form suitable for evaluation of multiple-process laser thermal damage effects and for comparison between numerical models and histologic results.

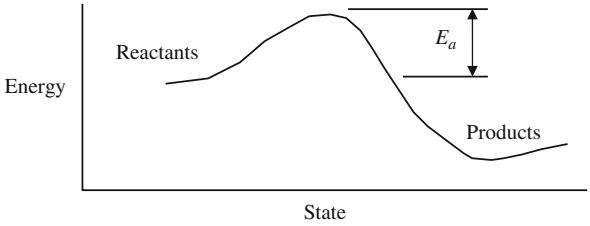

Fig. 13.14 Energy-state diagram. Reactants surmount energy barrier E_a to transition to products

Reaction Product Formation Rates

The basis for rate process models of thermal damage may be obtained from chemical reaction kinetics. In a typical reaction process, thermally active reactants jump over an energy barrier to form products, as illustrated in Fig. 13.14. In the figure, E_a is the energy barrier in Eq. (13.27). The collision theory description of ordinary first order bi-molecular reaction kinetics (see, for example, [76]) holds that the reactants are activated by collisions; n^* are activated out of n total molecules, and the probability of activation is:

$$\frac{n^*}{n} = e^{\left[\frac{-E_a}{RT}\right]} \tag{13.28}$$

In such a process, activated reactants are considered to form an activated "complex" which may either relax to inactivated single reactants or progress to form product molecules. The complex has some of the properties of an ordinary molecule and is at least temporarily stable. For reactant molecules A and B the activated complex is $[AB]^*$, and the sequence of formation is:

$$\text{Reactants} \quad A + B \underset{k_b}{\overset{k_a}{\rightleftarrows}} [AB]^* \xrightarrow{k} \text{Products} \tag{13.29}$$

The overall reaction velocity, $k\,[\mathrm{s}^{-1}]$, determines the rate of formation of product and is related to the equilibrium constant for formation of the activated complex, K^*, by:

$$k = \frac{RT}{Nh_P} K^* \tag{13.30}$$

where

$$K^* = e^{\frac{-\Delta G^*}{RT}}$$

and here N is Avogadro's number (6.023×10^{23}), h_P is Planck's constant (6.627×10^{-34} [J - s]), and ΔG^* is the Gibb's free energy of formation of activated complex [J·mole^{-1}]. As mentioned in the previous section, the free energy of formation is given by:

$$\Delta G^* = \Delta H^* - T\Delta S^* \tag{13.31}$$

where ΔH^* is the enthalpy of activation [J · mole^{-1}] and ΔS^* is the entropy of activation [J · mole^{-1} · K^{-1}]. The activation entropy is not calculable except for the simplest possible reactions in rarified gases, and is therefore usually determined from experimental measurements of the reaction velocity and activation enthalpy. The activation enthalpy, ΔH^*, is determined from the observed activation energy, E_a by:

$$\Delta H^* = E_a - i\,RT \tag{13.32}$$

where i is 1 for first-order reactions in solution and gases, 2 for second order, and 3 for third order reactions.

Unimolecular Process Descriptions

Thermal damage in tissue is a unimolecular process – tissue constituents transition from the native state to the damaged state. Absolute reaction rate theory can also be used to explain the rate of formation for this process if we assume that a time lag exists between molecular activation and denaturation [76]. During this time lag, the molecules may either denature or relax back to the native state, as illustrated in Fig. 13.15. Here, ΔH is the enthalpy (i.e. internal thermal energy) difference between native state and denatured molecules. The relative barriers are such that in the thermal damage of tissue, ΔH^*, is almost always smaller than ΔH. So, the activation process may be regarded as reasonably likely, and the probability of denatured tissue relaxing back to native state tissue is near enough to zero that it may be regarded as the impossible event in the absence of an energy-consuming healing process. The rate of damage formation is then proportional to only those molecules that remain activated. For a unimolecular process in the native state C, having an activated state, C^*, with velocity constants k_a, k_b, and k_3:

$$C + C \underset{k_b}{\overset{k_a}{\rightleftarrows}} C + C^* \tag{13.33a}$$

$$C^* \xrightarrow{k_3} \text{Damaged Molecules} \tag{13.33b}$$

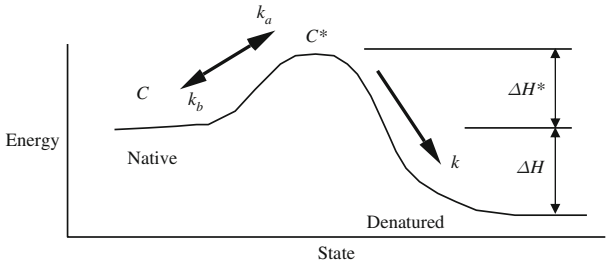

Fig. 13.15 Energy-state diagram for unimolecular reaction with energy barrier ΔH^*. Transition to denatured (damaged) tissue constituents occurs at overall reaction speed k

For this process, the rate of disappearance of native state molecules, $[C]$, is given by:

$$-\frac{d[C]}{dt} = k_3 \left[C^*\right] \tag{13.34}$$

where the bracket is used to indicate molar concentration. Generally $[C^*]$ is neither known nor calculable; however, at sufficiently low concentrations of C^* the steady state principle asserts that for short-lived activated states the rate of formation can be considered equal to the rate of disappearance. So the activated state, $[C^*]$, forms at a rate $k_a[C]^2$, relaxes back to inactivated at rate $k_b[C][C^*]$, and denatures at rate $k_3[C^*]$. Consequently:

$$k_a [C]^2 = k_b [C]\left[C^*\right] + k_3\left[C^*\right] \tag{13.35a}$$

$$\left[C^*\right] = \frac{k_a [C]^2}{k_b [C] + k_3} \tag{13.35b}$$

Of course, we seek an overall reaction velocity, k, which relates $[C]$ to its rate of disappearance:

$$-\frac{d[C]}{dt} = k [C] \tag{13.36}$$

There are two limiting cases for Eq. (13.35b). First, the concentration of remaining undamaged material, $[C]$, may be large enough that deactivation at k_b dominates the k_3 pathway, so $[C^*] \cong [C]k_a/k_b$ for which the overall formation rate, $k = k_3(k_a/k_b)$ and a first order process results. Second, if the remaining undamaged material concentration, $[C]$, is small, $k_3 >> k_b[C]$ and the process is second order since from Eq. (13.35a) $k \cong k_a/k_3[C]$. In liquid phase systems with appreciable concentrations of native state molecules the first condition should apply, so the first order approximation applies. After a long time of exposure at damaging temperatures such that $[C]$ is very small, $k_3 >> k_b[C]$ and a second order process results:

$$-\frac{d[C]}{dt} = k [C]^2 \tag{13.37}$$

where for simplicity the $[C]$ dependence has been removed from k: $k \cong k_a/k_3$. At such low concentrations the damage process is saturated, so we may ignore that case for the present.

Equation (13.36), then, is a Bernoulli differential equation with the solution:

$$C(\tau) = C(0)\, e^{\left\{-\int_0^\tau k\, dt\right\}} \tag{13.38}$$

Equations (13.30) and (13.31) may be used to relate k to ΔH^* and ΔS^*. It should be noted at this point that the energy barrier, E_a, (Fig. 13.14) is in fact $\Delta H^* + RT$

(Eq. 13.32); however, in practice $\{\Delta H^* \cong 5 \times 10^5\} >> \{RT \cong 3 \times 10^3\}$, so little error results from assuming that $E_a \cong \Delta H^*$. This approximation may be used to obtain:

$$k = \left(\frac{RT}{Nh_P}\right) \quad e^{\left[\frac{\Delta S^*}{R}+1\right]} \quad e^{\left[\frac{-E_a}{RT}\right]} \cong \left(\frac{RT}{Nh_P}\right) \quad e^{\left[\frac{\Delta S^*}{R}\right]} \quad e^{\left[\frac{-\Delta H^*}{RT}\right]} \tag{13.39a}$$

$$k \cong A\, e^{\left[\frac{-\Delta H^*}{RT}\right]} \tag{13.39b}$$

The term in parentheses in Eq. (13.39a) suggests that the pre-exponential factor, A, is not constant but is in fact temperature dependent. However, the linear dependence of A on temperature is extremely weak – especially when compared to the exponential dependence in the final term – and its effect is negligible, so that for all practical purposes A may be treated as a constant over the temperature ranges of interest.

Arrhenius Formulations in Thermal Damage Studies.

A more useful form of Eq. (13.27) may be obtained by recasting the result into a volume fraction model. In this formulation, as above, C signifies the remaining concentration of native state (undamaged) tissue constituent molecules. Therefore, the physical significance of the traditional damage measure, Ω, is the logarithm of the ratio of the original concentration of native tissue to the remaining native state tissue at time τ:

$$\Omega(\tau) = \ln\left\{\frac{C(0)}{C(\tau)}\right\} = \int_0^\tau A\, e^{\left[\frac{-E_a}{R\,T(t)}\right]}\, dt \tag{13.40}$$

where the frequency factor, A, and energy barrier, E_a, are related to the activation enthalpy and entropy, ΔH^* and ΔS^*, by Eq. (13.39a).

This form of the damage integral has the advantage that it is more easily compared to quantitative pathologic endpoints such as birefringence loss, collagen damage, or cell survival in culture. Using this description, direct comparisons can be made between computer models of transient thermal fields, $T(x,y,z,t)$, integrated over time and the measured histologic damage. A set of coefficients, A and $E_a \cong \Delta H^*$, is required for each damage process considered in the computer model. For tissue damage processes studied to date, A varies from about 10^{40} to 10^{105} [s^{-1}] while E_a ranges from about 1×10^5 to 9×10^5 [$J \cdot mole^{-1}$]. Each damage process is then allowed to progress in parallel, driven by the calculated thermal field. This formulation assumes that the individual processes are thermodynamically independent, a reasonable description for identifiable thermal damage processes. The concentration of each of the damage markers, $C(\tau)_i$, is accumulated; and a distributed field description of the predicted histologic endpoint is generated – for example, the boundary of thermally induced birefringence loss can be predicted. The model predictions are then suitable for comparison to histologic results.

Functional Behavior of the Damage Model

The characteristic behavior of the kinetic damage model is that below a threshold temperature the rate of damage accumulation is negligible, and it increases precipitously when this value is exceeded. This behavior is to be expected from the exponential nature of the function. For purposes of discussion, it is useful to define the critical temperature, T_{crit}, as the temperature at which the damage accumulation rate, $d\Omega/dt$, is 1:

$$\frac{d\Omega}{dt} = 1 = A\, e^{\left[\frac{E_a}{R\,T_{\text{crit}}}\right]} \tag{13.41}$$

so,

$$T_{\text{crit}} = \frac{E_a}{R\ \ln\{A\}}$$

For a process with (arbitrary) representative coefficients of $A = 1.0 \times 10^{75}$ and $E_a = 5 \times 10^5$, the critical temperature is 74.8°C. Figure 13.16 illustrates the damage accumulation rate dependence on temperature for the hypothetical example process. Note that the plot is converted from [K] to [°C] for the figure. In Fig. 13.17 the damage accumulation rate is plotted vs. 1/T [K^{-1}] for comparison.

Constant temperature exposures of the example process will result in a decrease in concentration of native state material depending on the time of exposure. A constant temperature exposure reduces the integral of Eq. (13.40) to a simple multiplication. Figure 13.18 shows the remaining concentration for this hypothetical example damage process for constant temperature exposures of time $\tau = 0.1$, 1.0, and 10 s. The concentration may be seen to gradually decrease with increasing temperature for fixed exposure times, as expected; the strong exponential nature of the process is evident as well. Applying this model framework relies heavily on identifying independent damage processes that can be quantitatively measured.

From plots like Fig. 13.18, estimates of A and E_a may be made from the $\Omega = 1$ line (i.e. $C(\tau) = 36.8\%$). Each curve will give one point on an Arrhenius plot ($\ln\{\tau\}$ vs. $1/T$) where $\Omega = 1$:

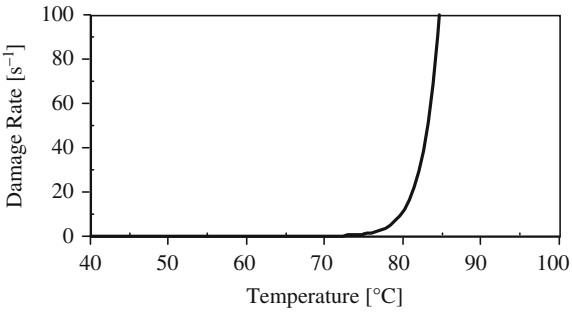

Fig. 13.16 Damage accumulation rate, $d\Omega/dt$, vs. temperature for the example process; $A = 1.0 \times 10^{75}$ and $E_a = 5 \times 10^5$

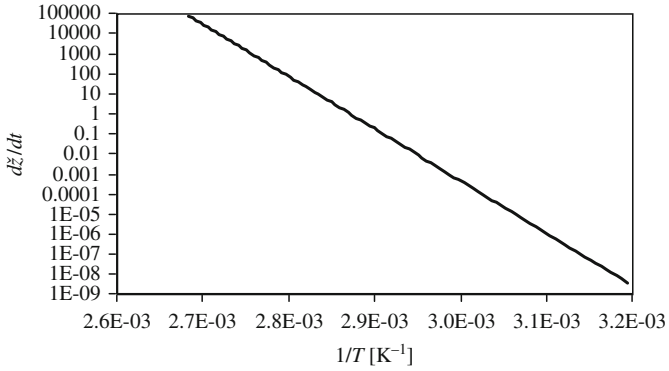

Fig. 13.17 Damage accumulation rate, $d\Omega/dt$, vs. $1/T\,[\mathrm{K}^{-1}]$ for the hypothetical example process; $A = 1.0 \times 10^{75}$ and $E_a = 5 \times 10^5$

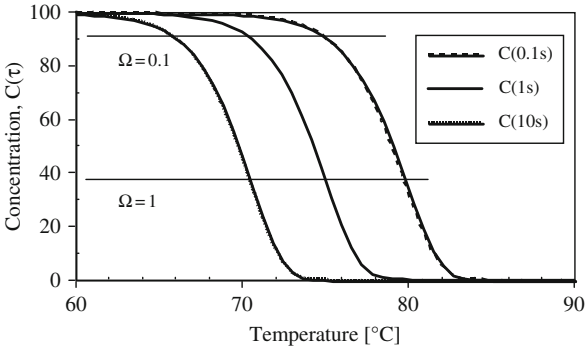

Fig. 13.18 Remaining undamaged tissue, $C(\tau)$, vs. T [°C] for the hypothetical example process; $A = 1.0 \times 10^{75}$ and $E_a = 5 \times 10^5$ for exposure times of 0.1, 1 and 10 s. Lines for $\Omega = 0.1$ and $\Omega = 1$ are also shown. At $\Omega = 10C(\tau) = 4.5 \times 10^{-3}$ and is not resolvable on the plot

$$\ln\{\tau\} = \left(\frac{E_a}{R}\right)\frac{1}{T} - \ln\{A\} \tag{13.42}$$

Estimates of A and E_a may then be obtained from a least-squares regression fit to the line of Eq. (13.42). Note the necessity of using exposure times that span several orders of magnitude in order to separate the curves sufficiently to give acceptable accuracy in the determination of the kinetic coefficients.

Though the damage parameter, Ω, cannot be measured directly in histologic section, often a clearer picture of the functional behavior can be obtained from it. The exponential dependence of damage on the inverse of absolute temperature means that the temperature required to obtain comparable damage levels is quite sensitive to time of exposure. For example, we may define a threshold temperature, T_{TH}, as the temperature at which the damage parameter, Ω, is 1 for a given duration, τ. Rearranging Eq. (13.42) gives the threshold temperature:

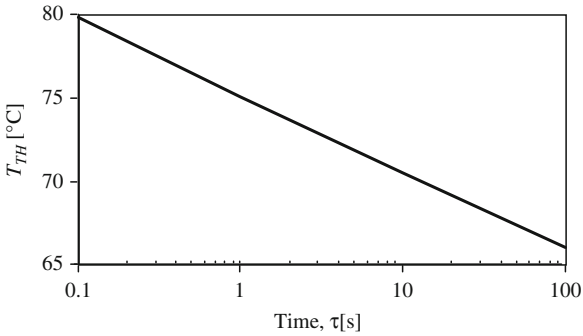

Fig. 13.19 Threshold temperature T_{TH} [°C] for the hypothetical example process; $A = 1.0 \times 10^{75}$ and $E_a = 5 \times 10^5$ vs. τ

$$T_{TH} = \frac{E_a}{R\ [\ln\{\tau\} + \ln\{A\}]} \tag{13.43}$$

Figure 13.19 is a plot of the threshold temperature as a function of duration for the example damage process of Figs. 13.16 and 13.18. Note that threshold temperature is approximately exponentially dependent on duration, as expected, with (in this case) a slope of about −4.65°C/decade. So, while 79.5°C is sufficient to result in $\Omega = 1$ (i.e. 63.2% damage) at 0.1 s, 102.3°C would be required for a 1 μs exposure for this process.

13.3.3.2 Experimental Determination of Rate Process Coefficients

Thermal damage kinetic coefficients are usually determined from constant temperature exposures of relatively long duration. Threshold damage results are selected out of a set of damaged tissue samples for analysis from which estimates of A and E_a are obtained.

Constant Temperature Exposures

Because of the sensitivity of the damage integral to small changes in temperature, the typical approach in obtaining A and E_a is to expose the tissue to a constant temperature, identify experiments in which the damage, $\Omega = \ln\{C(0)/C(\tau)\}$ is known and obtain A from the intercept and E_a from the slope of an Arrhenius plot of $\ln(\tau)$ vs. $1/T$ for the those experiments. If the temperature is held constant at T (K) Eq. (13.40) becomes:

$$\ln\{\tau\} = \left(\frac{E_a}{R}\right)\frac{1}{T} - \ln\{A\} + \ln\{\Omega\} \tag{13.44}$$

For experiments with $\Omega = 1$, $\ln\{\Omega\} = 0$ and a linear regression fit to the data plotted on $\ln\{\tau\}$ vs. $1/T$ axes gives the desired coefficients: intercept $b = -\ln\{A\}$ and slope $m = (E_a/R)$.

For constant temperature experiments in which Ω is known but not equal to 1, a simple re-arrangement of Eq. (13.44) yields the values required for an Arrhenius plot. In Eq. (13.45) the time of exposure for an equivalent experiment that would have $\Omega = 1$ at the experiment temperature T, i.e. τ_1, is simply related to the actual experiment conditions – Ω, T and τ – by:

$$\ln\{\tau\} - \ln\{\Omega\} = \ln\{\tau_1\} = \left(\frac{E_a}{R}\right)\frac{1}{T} - \ln\{A\} \tag{13.45}$$

In practice, one then plots $\ln\{\tau_1\}$ vs. $1/T$ (K^{-1}) for all useful data points and fits a linear regression line to determine the process coefficients from the slope and intercept.

The usual experimental method is to expose thin slices of tissue to constant temperature in a water bath, by surface application of heated water [72, 77] or on a heated metallic plate for desired time intervals. Table 13.4 lists rate coefficients obtained in various experiments. When using the kinetic models and measured coefficients, it is imperative that an adequate description of the particular end point be given. This is because different end points in the same tissue will have widely varying critical temperatures and damage accumulation rates. For example, in Table 13.4 in addition to the variation in tissues, the thermal damage histologic end points in the various studies differ.

Retina

The measurements of Welch and Polhamus [78] used the diameter of the edge of the visible lesion formed in rhesus monkey retina in vivo under argon laser irradiation as the end point. The temperatures were not measured directly, but were determined in separate experiments on retinas in which a correlation between temperature and radius was established using micro-thermocouples (about 5 μm in diameter) advanced from the posterior surface of the eye to a point just below the retina. The correlates were used to estimate the retinal temperature given laser beam power for durations between 0.1 and 10 s. The critical temperature for these coefficients is 56.0°C.

Takata et al. [79] have used a similar decision criterion for retinal damage for shorter exposure times. They fit the data with three sets of coefficients because a single first order model was not sufficient. It would appear that several parallel damage processes were at work in their study, thus a set of coefficients was required – the usual case is that there will be "breakpoints" in the Arrhenius plots, and the regions require different coefficients to fit the data. The critical temperature for the high temperature set of their coefficients is 59.9°C.

Birngruber et al. [80, 81] estimated a frequency factor and activation energy from consideration of the thermodynamics of protein and enzyme denaturation processes. Their estimates have a critical temperature of 74.5°C.

Skin

The end point for $\Omega = 1$ in the original studies of Henriques and Moritz corresponded to a continuum of cascaded effects [72, 74]. In their study the skin of pigs

Table 13.4 Experimentally determined Arrhenius rate coefficients

Source/process	Damage process coefficients			Notes
	A (s^{-1})	E_a (J/mole)	T_{crit} (°C)	
Heat Shock Proteins				
Beckham [86]	6.90×10^{282}	1.74×10^{6}	48.2	
Cell Death				
Sapareto [85]	2.84×10^{99}	6.18×10^{5}	51.4	CHO Cells, ≥ 43 °C
Skin				
Henriques [75]	3.1×10^{98}	6.28×10^{5}	59.9	Not recommended
Diller [82, 87]	1.3×10^{95}	6.04×10^{5}	58.5	Recommended (same data)
Weaver [83]	2.185×10^{124}	7.82×10^{5}	55.4	$T \leq 50$°C
	1.823×10^{51}	3.27×10^{5}	60.1	$T > 50$°C
Wu [88]	3.1×10^{98}	6.27×10^{5}	59.4	$T \leq 53$°C
	3.1×10^{98}	$6.27 \times 10^{5} - 5.1 \times 10^{5}$ $(T-53)$		$T > 53$°C
Fuggitt [89]	3.1×10^{98}	6.28×10^{5}	59.9	$T \leq 55$°C
	5.0×10^{45}	2.96×10^{5}	65.2	$T > 55$°C
Takata [90]	4.322×10^{98}	4.18×10^{5}	64.6	$T \leq 50$°C
	9.389×10^{104}	6.69×10^{5}	59.7	$T > 50$°C
Retinal Damage				
Welch [78]	3.1×10^{99}	6.28×10^{5}	57.6	Damage
Takata [79]	4.322×10^{64}	4.18×10^{5}	64.6	$T \leq 50$°C (Coagulation)
	9.389×10^{104}	6.69×10^{5}	59.7	$T > 50$°C
Vassiliadis [91]	9.95×10^{43}	2.90×10^{5}	71.1	Coagulation
Birngruber [80, 81]	1×10^{44}	2.93×10^{5}	74.7	
Collagen Changes				
Miles [92]	1.60×10^{137}	8.59×10^{5}	53.9	In lens capsule
Jacques [93]	7.35×10^{64}	4.251×10^{5}	69.2	Contraction of mouse dermis
Maitland [39]	1.77×10^{56}	3.676×10^{5}	68.2	Rat tail birefringence loss
Pearce [77]	1.606×10^{45}	3.06×10^{5}	80.4	Rat skin birefringence loss
Muscle				
Gaylor [94] See also: Toner [95] or Lee [96]	2.9×10^{37}	2.4×10^{5}	61.5	Cell membrane rupture
Jacques [97]	2.94×10^{39}	2.596×10^{5}	70.4	Myocardium whitening ~ birefringence loss

Table 13.4 (continued)

Source/process	Damage process coefficients			Notes
	A (s^{-1})	E_a (J/mole)	T $_{crit}$ (°C)	
Agah [98]	3.0×10^{23}	1.62×10^5	87.3	Optical properties changes
Erythrocytes				
Moussa [51]	6.8×10^{36}	2.49×10^5	80	Membrane denaturation
Lepock [52]	7.6×10^{66}	4.55×10^5	82.2	Hemoglobin coagulation
Flock [99]	1×10^{31}	2.12×10^5	84	Membrane denaturation
Egg				
Yang [84]	3.8×10^{57}	3.85×10^5	76	Egg albumin, whitening
Yang [84]	3.05×10^{56}	3.89×10^5	86.6	Egg yolk, whitening
Liver				
Jacques [100]	5.51×10^{41}	2.769×10^5	73.4	Whitening, pig liver
Mathewson [101]	2.09×10^{33}	2.219×10^5	74.7	Necrosis, rat liver
Prostate				
Jacques [102]	2.08×10^{27}	1.866×10^5	83.6	Whitening
Skinner [103]	3.8×10^{57}	3.85×10^5	76	Whitening, absorption coeff.
Kidney				
He [104]	1.48×10^{60}	3.996×10^5	73.7	Whitening, pig kidney
	3.3×10^{38}	2.569×10^5	75.2	Delayed necrosis
Pop [105]	5.73×10^{34}	2.404×10^5	88	Electrical conductivity
	5.85×10^{28}	2.023×10^5	94.2	Electrical permittivity

Coefficients are arranged by damage or tissue type and in the order of Increasing T_{crit}. References are listed by first author.

was exposed, in vivo, to flowing water at a controlled temperature for exposure times varying over several orders of magnitude. They calibrated their coefficients so that $\Omega = 0.5$ corresponded to the onset of erythema (characterized as "first degree" in their paper). Then $\Omega = 1$ corresponded to a "second degree," or a partial thickness, burn, and $\Omega = 10^4$ to a full thickness, or "third degree," burn. Their published coefficients, $A = 3.1 \times 10^{98}$ and $E_a = 6.28 \times 10^5$, have a critical temperature of 59.7°C. Interestingly, although these coefficients have been used for many years by numerous investigators, they do not fit the original data very well. In a later analysis, Diller and Klutke applied linear regression to their original data for temperatures less than 52°C – for which $A = 1.3 \times 10^{95}$ and $E_a = 6.04 \times 10^5$ – and if the data point at

52°C is included, $A = 0.865 \times 10^{95}$ and $E_a = 6.03 \times 10^5$, virtually the same result [82]. In any event, these new coefficients should be used in future work as they fit the original data much better than those originally published in 1947.

Weaver and Stoll [83] used similar criteria to the original 1947 studies and applied two sets of coefficients, as in Table 13.4 (the upper values are applicable above 50 °C) to match the experimental data. The critical temperature for their highest temperature coefficient set is 59.4°C.

Egg White and Egg Yolk

Yang et al. [84] exposed egg white and egg yolk to constant temperature (± 0.2°C) in a water bath for varying exposure times. Coagulation was defined as the onset of whiteness (coagulum formation due, apparently, to an increase in scattering in the clear liquid egg white) observed by the naked eye. Water bath temperatures ranged from 60 to 90°C in 4°C increments. At each temperature the time to threshold (onset of observable change) was measured and plotted in accordance with Eq. (13.44) and rate coefficients determined from linear regression, as described. Approximately 3–5 s were required to obtain whitening in the egg white at 70°C; while in the egg yolk 82°C was required at the same exposure time. The Table 13.4 values have a critical temperatures of 76.0°C for egg white and 86.6°C for egg yolk.

Birefringence Loss in Collagen

Birefringence loss in rat skin collagen was measured at temperatures between 40 and 90°C in 5°C increments for times ranging from 120 to 6000 s [77]. The gross extracted skin was wrapped in aluminum foil and immersed in a water bath. The heated samples were sectioned diagonally to increase their area, mounted on glass slides and stained (H&E) for analysis (see Fig. 13.9). The relative intensity of birefringence was determined using the exposure meter on the microscope camera in the "spot" mode: assuming that reciprocity applies, the intensity is the inverse of the indicated exposure time. This approach was necessary because the birefringence image is very low intensity: normal film exposure times required range up to 20 s in ASA 64 film. Intensity was calculated from data normalized by the background light intensity for each microscope slide, I_0. Relative birefringence intensity was then calculated by subtracting the fully denatured birefringence intensity, I_d, from the specimen intensity, I_s, and native state (undamaged) intensity, I_n, with all intensities individually normalized by I_0 before the calculation:

$$B = \frac{I_s - I_d}{I_n - I_d} \tag{13.45b}$$

A typical set of histologic sections from these data was presented in Fig. 13.5. The $\Omega = 1$ values were determined from the plot similar to Fig. 13.18 in order to calculate A and E_a. For the estimated $\Omega = 1$ points in this data set, $\ln\{\tau\} = 36,753\,(1/T) - 104$ with $r^2 = 0.900$, so the calculated values are: $A = 1.606 \times 10^{45}(s^{-1})$ and $E_a = 3.06 \times 10^5(\mathrm{J \cdot mole^{-1}})$, and $T_{\mathrm{crit}} = 80°\mathrm{C}$.

Deriving Damage Coefficients from Survival Curves

Another format typically used to present thermal damage data is the cell survival curve, derived from cell culture experiments. The simplest format in which to calculate A and E_a is a plot of surviving fraction *vs*. time at a fixed temperature. In that case the surviving fraction is simply $C(\tau)$, and a straight forward calculation can be done for $\Omega(\tau)$, from which A and E_a can quickly be extracted by curve fitting.

Alternately, the time required for the population to decrease by a factor of e^{-1} may also be used; see Fig. 13.20 [85]. D_0 is the time for the colony formation rate to decrease by e^{-1}:

$$\frac{S}{N_0} = e^{\frac{t_0 - t}{D_0}} \tag{13.46}$$

where $N_0 =$ the initial cell count measured at time t_0, and $S =$ surviving cell count at time t.

This parameter is plotted for asynchronously dividing Chinese Hamster Ovary (CHO) cells, and for CHO cells in the G1 phase in Fig. 13.20. The G1 phase is cell

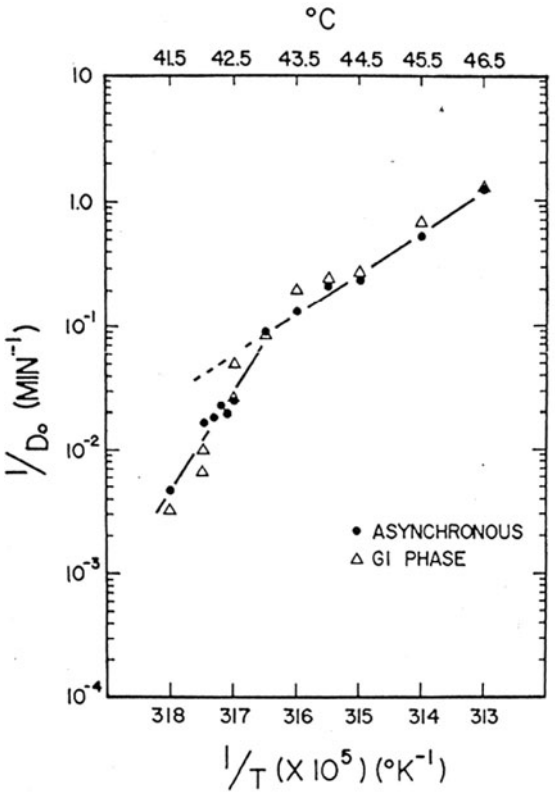

Fig. 13.20 Cell survival curve for Chinese Hamster Ovary (CHO) cells, a standard tumor cell line (reproduced from [85] and used by permission). The plot is $1/D_0$ [minutes^{-1}] vs. $1/T$ [K^{-1}]. Note the breakpoint at 43°C

growth immediately after a new cell is produced. The asynchronous cells have a random distribution of growth phases. CHO cells are common model cell lines used in tumor hyperthermia studies. By Eq. (13.46) the relationship for D_0 reduces to:

$$\ln\left\{\frac{C(0)}{C(\tau)}\right\} = 1 = \int_0^{D_0} A\, e^{\left[\frac{-E}{RT}\right]}\, dt \tag{13.47}$$

from which it may quickly be determined that:

$$\ln\{D_0\} = \frac{E}{RT} \; - \; \ln\{A\} \tag{13.48}$$

and the Arrhenius plot may be constructed as previously described. For the asynchronous CHO cells in this data set at temperatures above the break point (43°C) $A = 2.84 \times 10^{99}(\mathrm{s}^{-1})$ and $E_a = 6.18 \times 10^5[\mathrm{J \cdot mole}^{-1}]$, and $\mathrm{T_{crit}} = 51.4°\mathrm{C}$.

The usual damage prediction in hyperthermia studies is to express the exposure in terms of "Cumulative Equivalent Minutes" of exposure at the breakpoint temperature, typically very near 43°C in most tissues. The goal in those studies is to ensure cell death in the tumor, so the threshold for "success" is usually taken to be CEM = 30–60 min, depending on the application:

$$CEM\,43 = \sum_{i=1}^{N} R^{(43-T_i)}\, t_i \tag{13.49}$$

where t_i = the time of exposure [minutes] at temperature T_i [°C] and R is derived from a plot like Fig. 13.20. For most tissues above the breakpoint $R \simeq 0.5$, and can be calculated from:

$$\ln\{R\} = \frac{\ln\left\{\frac{D_0(T_{\mathrm{break}})}{D_0(T)}\right\}}{(T_{\mathrm{break}} - T)} \tag{13.50}$$

Example 13.7: This example derives Arrhenius coefficients from the CHO cell survival curve of Fig. 13.20 for temperatures below the break point, 43°C.

Solution:

(1) Reading lower temperature values for synchronous CHO cells from the plot:

T (°C)	T(K)	$D_0{}^{-1}$ (min^{-1})	D_0(s)	Ln{D_0}
43	316.2	0.09	667	6.503
42.5	315.7	2.6×10^{-2}	2308	7.744
42	315.2	1.6×10^{-2}	3750	8.230
41.7	314.9	4.8×10^{-3}	12,500	9.433

(2) Linear regression fit, $\ln\{D_0\}$ vs. T^{-1}

$$\ln\{D_0\} = 206,035\left[\frac{1}{T}\right] - 645.1$$

(3) $\ln\{A\} = 645.1$ means that $A = 1.46 \times 10^{280}$ (is this a frightening number, or what?)
(4) $E/R = 206,035$ means that $E = 1.71 \times 10^6[\text{J} \cdot \text{mole}^{-1}]$.

In practice, Eq. (13.49) is the discrete form of a continuous integral for time-varying temperatures. It should be noted that the *CEM43* damage calculation yields only an equivalent time of exposure and not a damage probability result. A *CEM43* value can be converted into a probability calculation if $D_0(43)$ is known for the tissue, however, by application of Eq. (13.46).

In summary, Fig. 13.21 compares several of the representative processes selected from Table 13.4 in terms of their relative rates of damage accumulation vs. temperature.

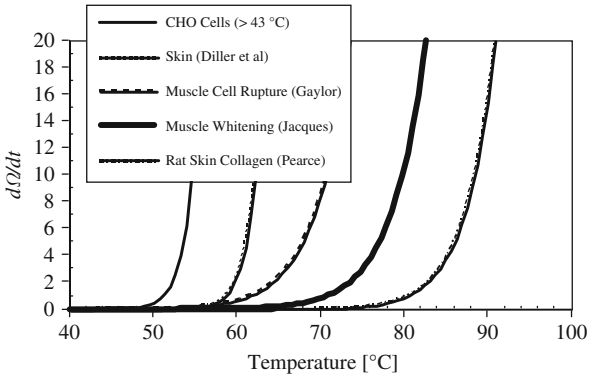

Fig. 13.21 Comparison of five representative rates of damage accumulation, $d\Omega/dt$, based on coefficients selected from Table 13.4, arranged in order of increasing critical temperature

Transient Thermal History Experiments

Problems with the standard constant temperature approach to determining A and E_a are that: (1) with only very few exceptions, the tissue must be excised to perform the experiments, disrupting its normal blood perfusion and activating autolytic (post mortem degeneration and necrosis) processes; (2) no exposure is truly constant temperature, and rise time segments must necessarily be short compared to the total exposure time in order to be negligible; and (3) the methods are essentially impossible to use in laser damage studies since constant temperature exposures are not possible to obtain and the typical small spot sizes mean that substantial thermal gradients confound reliable determination of the temperature history. Working with transient thermal data adds a high level of uncertainty to the damage coefficients

since the time of exposure is problematic. Nevertheless, estimates of rate coefficients can be made upon which treatment protocols can be evaluated.

Here we present a new method specifically applicable to transient temperature heating cases [106]. While it does not address the small-spot, steep thermal gradient problem, the new method does solve the transient temperature exposure problem so that shorter exposures may be used in a data set, thus reducing the uncertainty in the estimated damage coefficients. We can rearrange Eq. (13.44) for $\Omega = 1$ experiments to see the basis for the method:

$$\ln\{A\} = \left(\frac{1}{RT}\right) E_a - \ln\{\tau\} \tag{13.51}$$

So, for a single constant temperature experiment resulting in $\Omega = 1$, we can plot a straight line in the $\ln\{A\}$ vs. E_a plane, with slope $1/RT$ and intercept $\ln\{\tau\}$. An ensemble of such lines from several experiments would intersect at the value of $\ln\{A\}$ and E_a that describe the thermal damage process under study. This exercise provides no new information for constant temperature experiments, of course.

However, such a plot does provide a convenient basis for analyzing transient heating experiments. For any experiment in which $C(t)$ or $\Omega(t)$ can be directly measured, determining A and E_a is a simple matter of curve fitting. Given an ensemble of experiments for which only the histologic endpoint $\Omega(\tau)$ and the transient history, $T(t)$, are known, we can assume values for $\ln\{A\}$ and E_a and calculate a relative "Cost" that is minimized when the integral of Eq. (13.40) is evaluated to calculate $\Omega\,(A, E_a)$:

$$\text{Cost} = \ln\left\{\frac{\int_0^\tau A\, e^{\left[\frac{-E_a}{RT(t)}\right]}\, dt}{\Omega\,(\tau)}\right\} \tag{13.52}$$

This is a standard optimization technique (Cost has no units). Here the "Cost" has been defined such that its magnitude approaches zero when the assumed values of $\ln\{A\}$ and E_a yield an integral equal to the measured $\Omega(\tau)$ value.

A two-dimensional gray-scale plot of the magnitude of the Cost on the $\ln\{A\}$ vs. E_a plane using hundreds of assumed values of A and E_a shows that the locus of points for which the |Cost| approaches zero is a straight line (see Fig. 13.22). In Fig. 13.22a, a hypothetical low-energy damage process with $A = 26.5 \times 10^9 [\text{s}^{-1}]$ and $E_a = 7 \times 10^4\,[\text{J} \cdot \text{mole}^{-1}]$ has been hypothetically heated in transient manner – i.e. with discrete temperatures shown in the plot calculated from a $t^{0.5}$ formula – including 2 s of cooling. The resulting damage value is $\Omega = 0.9$. In Fig. 13.22b the $\ln\{A\}$ vs. E_a plane is scanned for minima in the Cost, as calculated by Eq. (13.52) from the transient curve. In this figure the clarity of the functional behavior is enhanced by plotting the magnitude of $(\log_{10}\{1/\text{Cost}\})$. Other transient heating experiments will yield an ensemble of plots such as Fig. (13.22b), each with differing slope and intercept.

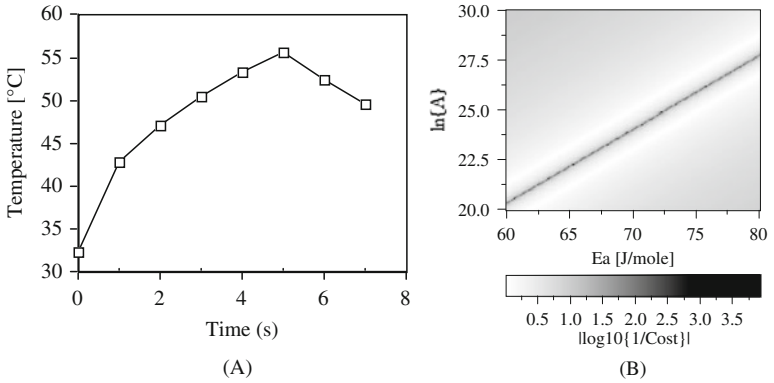

Fig. 13.22 Transient thermal history analyzed in the $\ln\{A\}$ vs. E_a plane. (**a**) Transient heating for a hypothetical process with $A = 26.5 \times 10^9$ and $E_a = 7 \times 10^4$ (linear in $t^{0.5}$) results in $\Omega = 0.9$. (**b**) Assuming values for A and E_a the transient temperature is integrated according to Eq. (13.52) and the inverse of Cost plotted in the plane. The locus of minima in Cost follow a straight line, the slope of which gives T_{eq} and the intercept $\ln\{\tau_{eq}\}$ for an equivalent constant-temperature experiment

The slope and intercept of the line of Cost minima in Fig. 13.22b contain extremely useful information. Referring to Eq. (13.51), the slope is $(1/RT_{eq})$ and the intercept is $\ln\{\tau_{eq}\}$, where T_{eq} and τ_{eq} are, respectively, the temperature and duration of an equivalent constant-temperature experiment for which $\Omega = 1$. It is then a simple matter to plot the ensemble of (T_{eq}, τ_{eq}) points on a standard Arrhenius plot, from which A and E_a are obtained in the ordinary fashion, i.e. from the slope and intercept of the linear regression line through them. In practice, the appropriate range to scan in the $\ln\{A\}$ vs. E_a plane can quickly determined by a coarse discrete scan of the values, followed by a fine scan to refine the estimate of T_{eq} and τ_{eq}.

This approach has the advantage over other curve fitting approaches that it preserves the underlying physics and reveals processes and relationships. It turns out to be quite critical that accurate values for the temperature be used to calculate the integral of Eq. (13.52). Consequently, an experiment design in which the temperature is uniform over a relatively large area is required so that spatial averaging can be used to reduce uncertainty in both the temperature and the quantitative damage measure. This excludes almost all laser spot approaches to damage process estimation. Note that it is neither necessary nor advantageous to have $\Omega = 1$ to make an Arrhenius plot when using this approach

Example 13.8 This example calculates the equivalent constant temperature experiment for the process described in Fig. 13.22. Here the hypothetical process has been integrated for the transient heating curve that resulted in $\Omega = 3.78$ for the hypothetical thermal damage process. The search plane was estimated using the strategy outlined in the text. The line of convergence in Fig. 13.22b has these points:

Cost	ln{A}	E (kJ/mole)
3.33×10^{-3}	62.75	181.4
4.05×10^{-3}	64.25	185.7
1.28×10^{-3}	65.58	189.6
5.23×10^{-3}	67.33	194.6
5.04×10^{-3}	68.75	198.8
3.70×10^{-3}	70.75	204.5
3.93×10^{-3}	72.25	208.9
2.73×10^{-3}	74.33	215.0

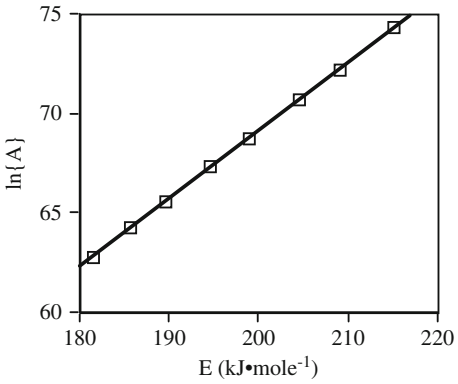

The fit for this line is: linear regression

$$\ln\{A\} = 0.345E\left(\text{kJ}\cdot\text{mole}^{-1}\right) + 0.201$$

So,

$$\frac{1}{R\,T_{eq}} = 0.345\times10^{-3}$$

$$\ln\left\{\tau_{eq}\right\} = -0.201$$

Or, $T_{eq} = 75.5°\text{C}$ and $\tau_{eq} = 0.818\,\text{s}$. For the original damage process ($A = 1 \times 10^{75}, E = 5 \times 10^5$) a constant temperature exposure of 0.818 s at 75.5°C results in $\Omega = 0.677$; close to $\Omega = 1$. Note that τ_{eq} is much shorter than the original experiment time of 5 s because the resulting damage in the simulated experiment gave Ω larger than 1. For experiments that have $\Omega < 1$, τ_{eq} will be longer than the experiment heating time. The difference between $\Omega = 0.677$ and the expected value of 1 is most likely due to an accumulation of round off errors: note how small 0.201 is compared to $\ln\{A\} = 172.7$ in Eq. (13.44), for example.

13.4 Summary

First order kinetic models for tissue damage are useful for predicting trends in laser damage experiments. Unfortunately, there are only a few damage processes for which the frequency factor and energy have been determined in situ – critical temperatures for known processes range from about 50 to 90°C. Nevertheless, these models can be used to make direct comparisons between numerical predictions of laser damage and histologic results, something that cannot, as yet, be achieved any other way. A very careful definition of the particular histologic end point is necessary. Also, to avoid the arbitrariness that characterizes many of the early damage studies, it is essential that a quantitatively measurable damage measure be identified. Birefringence intensity is one such variable; other excellent candidates include, for example, changes in optical properties such as the scattering or absorption coefficients on exposure to elevated temperatures.

In part because of the effects of biologic inhomogeneities and random fluctuations in tissue characteristics, and in part due to the difficulty of resolving small temperature differences, thermal damage data are inherently noisy. However, predicted boundaries in small spot size experiments compare favorably to those observed. This is probably due to the very steep thermal gradients typical of small spot experiments – that is, a rather large error in actual critical temperature may be swamped out by the very steep thermal gradient so that the location of the predicted damage contour may, in fact, agree fairly well with experimental histologic observation. Certainly, even though the results of a particular experiment may eventually prove impossible to duplicate in numerical models, a careful analysis of the trends which one would obtain from, say, changing beam power, spot size and duration can be studied in detail in the numerical model and on a spatial scale similar to that of microscopic observation. Also, the numerical model allows dissection of the transient development of thermal damage – something that cannot be achieved in any other way. So, while there are many uncertainties associated with kinetic models of thermal damage, they can be extremely illuminating and helpful in dosimetry planning.

References

1. Thomsen S. Pathologic analysis of photothermal and photomechanical effects of laser-tissue interactions. *Photochem. Photobiolog.*, 53(6):825–835 (1991).
2. Thomsen S. Identification of lethal thermal injury at the time of photothermal treatment. In: eds. G. Muller and A. Roggan (eds) *Intersitial thermotherapy*. SPIE, Bellingham, WA, pp. 459–467 (1995).
3. Thomsen S. Qualitative and quantitative pathology of clinically relevant thermal lesions. *SPIE Crit. Rev*., CR75:425–459 (2000).
4. Thomsen S. Non-thermal effects in thermal treatment applications of non-ionizing irradiation. *Proc. SPIE*., 5698:1–14 (2005).
5. Thomsen S and Coad JE. Developing clinically successful biomedical devices by understanding the pathophysiology of the target tissue: Insights from over 25 years at the microscope. *Proc. SPIE*., 6440:1–15 (2007).

6. Kumar,V, Abbas AK, Fausto N, and Mitchell RN. *Robbins basic pathology*. Saunders-Elsevier, Philadephia, 8th edition, pp. 1–224 (2007).
7. Lee H-C and Wei Y-H. Mitochondrial role in life and death of the cell. *J. Biomed. Sci*., 7:2–15 (2000).
8. Letal A and Scorrano L. Laying the foundations of programmed cell death. *Cell Death Differ.*, 13:1245–1247 (2006).
9. Chan D, Frank S, and Rojo M. Mitochondrial dynamics in cell life and death. *Cell Death and Differ.*, 13:680–684 (2006).
10. Coad JE. Thermal fixation: A central outcome of hyperthermic therapies. *Proc. SPIE*, 5698:15–22 (2005).
11. Metz CN. Fibrocytes: A unique cell population implicated in wound healing. *Cell. Mol. Life Sci.*, 60:1342–1350(2003).
12. Baum CL and Arpey CJ. Normal cutaneous wound healing: Clinical correlation with cellular and molecular events. *Dermatol. Surg*., 31:674–686 (2005).
13. Blakytny R and Jude E. The molecular biology of chronic wounds and delayed healing in diabetes. *Diabetic Med*., 23:594–608 (2006).
14. Williams P, Bannister LH, Berry MM et al. (eds). *Gray's anatomy. 38th international edition*. Churchill-Livingstone. Edinburg, pp. 1–2092 (1995).
15. Fawcett DW. *Textbook of histology*. Chapman and Hall, New York, 12th edition, pp. 1–964 (1994).
16. Ghadiallay FN. *Ultrastructural pathology of the cell and matrix*, Vols. 1 and 2. Butterworth-Heinemann, Boston, pp. 1–1450 (1997).
17. Alberts B, Johnson A, Lewis J et al. *Molecular biology of the cell.* Garland Science, New York, 4th edition, pp. 1–1463 (2002).
18. Junquiera LC and Carneiro J. *Basic histology: Text and atlas*. McGraw-Hill, Medical Publishing Division, New York, 11th edition, pp. 1–502 (2005).
19. Thomsen S. Practical pathology for engineers: How to do the job right the first time. *Proc. SPIE*, 4754:1–26 (2003).
20. Welch AJ and van Gemert MJC. (eds). *Optical-thermal response of laser-irradiated tissue.* Plenum, New York, pp. 1–925 (1995).
21. Niemz MH. *Laser-tissue interactions: Fundamentals and applications*. Springer, Berlin, 3rd edition (2004).
22. Thomsen S, Pearce JA, Randeri R, and Chan E. Determination of isotherms of thermal damage. *Proc. IEEE/LEOS*, 2295–2296 (1995).
23. Thomsen S. Mapping thermal injury in biologic tissues using quantitative pathologic techniques. *Proc. SPIE*., 3595:82–95 (1999).
24. LeCarpentier GL, Motamedi M, Rastegar S, and Welch AJ. Simultaneous analysis of thermal and mechanical events during cw laser ablation of biological media. *Proc. SPIE*, 1064: 107–113 (1989).
25. Verdaasdonk RM, Borst C, and van Gemert MJC. Explosive onset of continuous wave laser tissue ablation. *Phys. Med. Biol.*, 35:1129–1144 (1990).
26. Gijsbeers GHM, Selten FM, and van Gemert MJC. CW laser ablation velocities as a function of absorption in an experimental one dimentional model. *Lasers Surg Med.,* 11 :287–296 (1991).
27. Pearce JA and Thomsen S. Rate process analysis of thermal damage. In: AJ Welch and MJD van Gemert (eds) *Optical-thermal response of laser irradiated tissue*. Plenum, New York, pp. 561–606 (1995).
28. Protsenko DE and Pearce JA. Thermo-electrical numerical model of electrosurgical RF cutting. *Proc. SPIE*, 4247:203–209 (2001).
29. Nelson DL and M.M. Cox MM. *Lehninger principles of biochemistry*. W.H. Freeman and Co, New York, 4th edition, pp. 1–1119 (2005).
30. Guyton AG and Hall JE. *Textbook of medical physiology*. Saunders Elsevier, Philadelphia, 11th edition, pp. 1–1116 (2006).

31. Bray D. *Cell movements: From molecules to motility.* Garland, New York, 2nd edition, pp. 1–372 (2001).
32. Boal D. *Mechanics of the cell.* University Press. Cambridge, UK, pp. 1–406 (2002).
33. Ramachandran GN and Ramakrishan C. Molecular structure. In: Ramachandran GN and Reddi AH (eds) *Biochemistry of Collagen*. Plenum, New York. pp. 45–84 (1976).
34. Fleischmajer R, Olsen BR, and Kühn K. Biology, chemistry and pathology of collagen. *Annals NY Acad. Sci.*, 460:1–537 (1985) and 580:1–592 (1990).
35. Uitto J and Perejda AJ. *Connective tissue disease: molecular pathology of the extracellular matrix*. Marcel Decker, New York, pp. 1–563 (1987).
36. Chadwick DJ and Goode JA (eds). *The molecular biology and pathology of elastic tissues. Ciba symposium 192.* Wiley, New York, pp. 1–351 (1995).
37. Flory P and Garrett RR. Phase transitions in collagen and gelatin systems. *J. Am. Chem. Soc.*, 80:4836–4845 (1958).
38. Lim JJ. Transition temperature and enthalpy change dependence on stabilizing and destabilizing ion in the helix coil transition in native tendon collagen. *Biopolymers* 15:2371–2381 (1976).
39. Maitland DJ and Walsh JT Jr. Quantitative measurements of linear birefringence during heating of native collagen. *Lasers Surg. Med*., 20:310–318 (1997).
40. Yoshimura H, Viator JA, and Jacques SL. Relationship between damaged fraction and reflected spectra of denaturing tissues. *Lasers Surg. Med*., 37:308–313 (2005).
41. Schmidt SJ. Die Doppelbrechung von karyoplasma, zytoplasma und metaplasma. In: *Protoplasma-Monographien. Vol. II.* Verlag von Gebruder Borntraeger, Berlin, pp. 154–267 (1937).
42. Fisher E. The birefringence of striated and smooth muscles. *J. Cell. Comp. Physiol*., 23:11–130 (1944).
43. Peckham M and Irvin M. Myosin crossbridge orientation in demembranated muscle fibres studied by birefringence and X-ray diffraction measurements. *J. Mol. Biol*., 210:113–126 (1989).
44. Harris P and Heath D. Structure and function of vascular smooth muscle. In: *The human pulmonary circulation: Its form and function in health and disease.* Churchill Livingstone, New York, pp. 161–182 (1986).
45. Hulmes DJS, Miller A, Parry DAD et al. Crystalline regions in collagen fibrils. *J. Mol. Biol.*, 184:473–477 (1985).
46. Thomsen S, Pearce JA, and Cheong W-F. Changes in birefringence as markers of thermal damage in tissues. *IEEE Trans. Biomed. Eng.*, BME-36:1174–1179 (1989).
47. Thomsen S. Quantitative morphologic markers of laser thermal injury in cardiovascular muscle. *Proc. SPIE*, 1878:152–158 (1993).
48. Thomsen S, Jacques SL, and Flock S: Microscopic correlates of macroscopic optical property changes during thermal coagulation of myocardium. *Proc. SPIE*, 1202:2–11 (1990).
49. Thomsen S, Vijverberg H, Huang R, Schwartz J. Changes in optical properties of rat skin during thermal coagulation. *Proc. SPIE*, 1882:230–236 (1993).
50. Fielding CJ (ed). *Lipid Rafts and Caveolae: From membrane biophysics to cell biology*. Wiley-VCH, New York, pp. 1–294 (2006).
51. Moussa NA, Tell EN, and Cravalho EG. Time progression of hemolysis of erythrocyte populations exposed to supraphysiological temperatures. *Trans. ASME J. Biomech. Eng*., 101:176–184 (1979).
52. Lepock JR, Frey HE, Bayne H, Markus J. Relationship of hyperthermia-induced hemolysis of human erythrocytes to the thermal denaturation of membrane proteins. *Biochim. Biophys. Acta*, 980:191–201 (1989).
53. Bernardi, P, Scorrano L, Colonna R, Petronelli V, and Di Lisa F. Mitochondria and cell death: Mechanistic aspects and methodological issues. *Eur. J. Biochem*., 264:687–701 (1999).

54. Van Cruchten, S and Van den Brobeck W. Morphological and biochemical aspects of apoptosis, oncosis and necrosis. *Anat. Histol. Embryol*., 31:214–223 (2002).
55. Shoshan-Barmatz V, Israelson A, Brdiczda D, and Sheu SS. The voltage-dependent anion channel (VDAC): Function in intracellular signaling, cell life and cell death. *Curr. Pharm. Des*., 12:2349–2270 (2006).
56. Kim J-S, He L, Qian T, and Lemasters JJ. Role of the mitochondrial permeability transition in apoptotoc and necrotic death after ischemia/reperfusion injury o hepatocytes. *Curr. Mol. Med*., 3:527–235 (2003).
57. Anghieri LJ and Robert J. *Hyperthermia in cancer treatment.* CRC, Boca Raton (1986).
58. van der Zee J. Heating the patient: A promising approach? *Ann. Oncol*., 13:1173–1184 (2002).
59. Beynon, R and Bond JS. *Proteolytic enzymes.* University Press. Oxford, 2nd edition, pp. 1–340 (2001).
60. Thomsen S, Schwartz JA, Joseph R, Pearce JA, Rae B, and McMurray TJ. Temperatures associated with thermally induced red blood cell changes in tissues irradiated in vivo. *Proc. SPIE*, 2130:156–163 (1994).
61. Milleron RS and Bratton SB. "Heated" debates in apoptosis. *Cell. Mol. Life Sci*., 64:2329–2333 (2007).
62. Cohen IK, Diegelmann RF, and Lindblad WJ. *Wound healing: Biochemical and clinical aspects*. W.B. Saunders, Philadelphia, pp. 1–630 (1992).
63. Falanga V. *Cutaneous wound healing.* Martin Dinitz, London, pp. 1–484 (2001).
64. DiPietro LA and Burns AL. *Wound healing; Methods and protocols.* Humana, Totowa, NJ, pp. 1–453 (2003).
65. Grey JE and Harding KG. *ABC of wound healing.* Blackwell, Malden, MA, pp. 1–47 (2006).
66. Keenan JH and Keyes FG. *Thermodynamic properties of steam*, 1st edition, 19th printing. Wiley, New York (1948).
67. Van Wylen GJ. *Thermodynamics.* Wiley, New York (1964).
68. Reynolds WC. *Thermodynamics*. McGraw-Hill, New York (1970).
69. Torres JH, Motamedi M, Pearce JA, and Welch AJ. Experimental evaluation of mathematical models for predicting the thermal response of tissue to laser irradiation. *Appl. Opt.*, 32(4):597–606 (1993).
70. Brutsaert W. *Evaporation into the atmosphere: Theory, history and applications.* D. Reidel, Dordrecht, Holland (1982).
71. Yang D, Converse MC, Mahvi DM, and Webster JG. Expanding the bioheat equation to include internal water evaporation during heating. *IEEE Trans. Biomed. Eng*., 54(8):1382–11388 (2007).
72. Moritz AR and Henriques FC. Studies of thermal injury II. The relative importance of time and surface temperature in the causation of cutaneous burns. *Am. J. Pathol*., 23:695–720 (1947).
73. Moritz AR. Studies of thermal injury III. The pathology and pathogenesis of cutaneous burns: An experimental study. *Am. J. Pathol*., 23: 915–934 (1947).
74. Henriques FC and Moritz AR. Studies of thermal injury in the conduction of heat to and through skin and the temperatures attained therein: A theoretical and experimental investigation. *Am. J. Path*., 23:531–549 (1947).
75. Henriques FC. Studies of thermal injury V. The predictability and significance of thermally induced rate processes leading to irreversible epidermal injury. *Arch. Pathol*., 43:489–502 (1947).
76. Maron SH and Lando JB. *Fundamentals of physical chemistry*. McMillan, New York (1974).
77. Pearce JA, Thomsen S, Vijverberg H, and McMurray T. Kinetics for birefringence changes in thermally coagulated rat skin collagen. *Proc. SPIE*, 1876:180–186 (1993).
78. Welch AJ and Polhamus GD. Measurement and prediction of thermal injury in the retina of Rhesus monkey. *IEEE Trans. Biomed. Eng*., 31:633–644 (1984).

79. Takata AN et al. *Thermal model of laser induced eye damage*. Final Report, USAF School of Aerospace Medicine, Brooks AFB TX, Contract F41609-74-C-0005, IIT Research Institute, Chicago, IL (1974).
80. Birngruber R. Thermal modeling in biological tissue. In: F Hillenkamp, R Pratesi, and CA Sacchi (eds) *Lasers in biology and medicine,* Plenum, New York, pp. 77–97 (1980).
81. Birngruber R, Hillenkamp F, and Gabel VP. Theoretical investigations of laser thermal retinal injury. *Health Phys*., 48(6):781–796 (1985).
82. Diller KR, Pearce JA, and Valvano JW. Bioheat transfer, Chapter 4, Section 4. In: *CRC Handb. Therm. Eng.*, (cat. no. 9581), pp. 4–114, 4–187 (2000).
83. Weaver JA, and Stoll AM. Mathematical model of skin exposed to thermal radiation. *Aerospace Med*., 40(1):24 (1969).
84. Yang Y, Welch AJ, and Rylander HG. Rate process parameters of albumen. *Lasers Surg. Med*., 11:188–190 (1991).
85. Sapareto SA. *Physical aspects of hyperthermia*. G Nussbaum (ed). American. Institute of Physics, Chapter 1 (1982).
86. Beckham JT, Mackanos MA, Crooke C, Takahashi T, O'Connell-Rodwell C, Contag CH, and Jansen ED. Assessment of cellular response to thermal laser injury through bioluminescence imaging of heat shock protein 70. *Photochem. Photobiol.*, 79:76–85 (2004).
87. Diller KR and Klutke GA. *Accuracy analysis of the Henriques model for predicting burn injury*. Advances in Bioheat and Mass Transfer, AM. Soc. Mech. Eng., New York, 268 (1993).
88. Wu YC. *A modified criterion for predicting thermal injury*. Nat. Bur. Stand. Washington, District of Columbia (1982).
89. Fugitt CE. A rate process of thermal injury. Armed Forces Special Weapons Project No. AFSWP-606 (1955).
90. Takata AN. Development of criterion for skin burns. *Aerospace Med.*, 45:634–637 (1974).
91. VassiliadisA, Christian HC, and Dedrick KG. Ocular laser threshold investigations. *Aerospace Med. Rep*., F41609-70-0002 (1971).
92. Miles CA. Kinetics of collagen denaturation in mammalian lens capsules studied by differential scanning calorimetry. *Int. J. Biol. Macromol*., 15:265–271 (1993).
93. Jacques SL and Prahl SA. Modeling optical and thermal distributions in tissue during laser irradiation. *Lasers Surg. Med*., 6:494–503 (1987).
94. Gaylor DC. *Physical mechanism of cellular injury in electrical trauma*. Ph.D. Thesis, Department of Electrical Engineering, Massachusetts Institute of Technology (1989).
95. Toner M, Cravalho EG, Gaylor DC, and Lee RC. Cellular mechanisms of thermal injury in electrical trauma. *Proc. Ann. Conf. Eng. Med. Biol.*, 4:1505–1506 (1990).
96. Lee RC Gaylor DC, Prakah-Asante K, Bhatt D, and Israel DA. Skeletal muscle cell rupture by pulsed electric fields. *IEEE Eng. Med. Biol. Soc. Annu. Conf*., 712–714 (1987).
97. Jacques SL and Gaeeni MO. Thermally induced changes in optical properties of heart. *IEEE Eng. Med. Biol. Mag.* 11(Part 4/6):1199–1200 (1989).
98. Agah R, Gandjbakhche AH, Motamedi M, Nossal R, and Bonner RF. Dynamics of temperature dependent optical properties of tissue: dependence on thermally induced alteration. *IEEE Trans. Biomed. Eng.*, 43(8):839–846 (1996).
99. Flock ST, Smith L, and Waner MD. Quantifying the effects on blood of irradiation with four different vascular-lesion lasers. *Proc. SPIE*, 1882: 237–242 (1993).
100. Jacques SL, Newman C, and He XY. Thermal coagulation of tissues: Liver studies indicate a distribution of rate parameters not a single rate parameter describes the coagulation process. *Proc. Winter Annu. Meeting Am. Soc. Mech. Eng.* (1991).
101. Matthewson K, Coleridge-Smith P, O'Sullivan JP, Northfield TC, and Bown SG. Biological effects of intrahepatic neodymium:yttrium-aluminum-garnet laser photocoagulation in rats. *Gastroenterology*, 93:550–557 (1987).
102. Jacques SL, Motamedi M, and Rastegar S. Computer simulation of laser coagulation of prostate: A guide to dosimetry. *Am Soc. Lasers Med. Surg. Lasers Surg. Med.*, Suppl 5, abstract 311 (1993).

103. Skinner MG, Everts S, Reid AD, Vitkin IA, Lilge L, and Sherar MD. Changes in optical properties of *ex vivo* rat prostate due to heating. *Phys. Med. Biol*., 45:1375–1386 (2000).
104. He X, McGee S, Coad JE, Schmidlin F, Iaizzo PA, Swanlund DJ, Kluge S, Rudie E, and Bischof JC. Investigation of the thermal and tissue injury behaviour in microwave thermal therapy using a porcine kidney model. *Int. J. Hyperthermia*, 20:567–593 (2004).
105. Pop M, Molckovsky A, Chin L, Kolios MC, Jewett MA, and Sherar MD. Changes in dielectric properties at 460 kHz of kidney and fat during heating: Importance for radio-frequency thermal therapy. *Phys. Med. Biol*., 48:2509–2525 (2003).
106. Pearce JA and Thomsen S. Arrhenius model thermal damage coefficients for birefringence loss in rabbit myocardium. *Proc. ASME Int'l. Mech. Eng. Conf. Expos*., IMECE2003-41986 (2003).